Photochemical Stability of 5-Methylcytidine Relative to Cytidine: Photophysical Insight for mRNA

Therapeutic Applications

Sean J. Hoehn, † Sarah E. Krul, † Michael M. Pogharian, ‡ Erqian Mao, Carlos E. Crespo-Hernández*

Department of Chemistry Case Western Reserve University 44106 Cleveland, Ohio (United States)

AUTHOR INFORMATION

Corresponding Author

* E-mail: carlos.crespo@case.edu

 † these two authors contributed equally to this work

‡ participated as an undergraduate research assistant

ABSTRACT

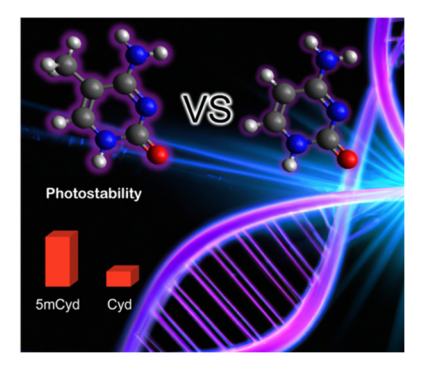
5-Methylcytidine (5mCyd) has recently been investigated with renewed interest for utilization in mRNA therapeutics. However, its photostability following exposure to electromagnetic radiation

has been overlooked. This Letter compares the photostability and excited state dynamics of 5mCyd

1

with those of the canonical RNA nucleoside, cytidine (Cyd) using steady-state and femtosecond transient absorption spectroscopy under physiologic conditions. 5mCyd is shown to have a 5-fold higher fluorescence yield and a 5-fold longer ${}^{1}\pi\pi^{*}$ excited state decay lifetime. Importantly, however, the excited state population in 5mCyd decays primarily by internal conversion, with a photodegradation rate 3 times smaller than in Cyd. In Cyd, the population of a ${}^{1}n\pi^{*}$ state with a lifetime of ca. 45 ps is implicated in the formation 6-hydroxycytidine and other photoproducts.

TOC GRAPHICS



KEYWORDS RNA, photochemistry, photostability, excited-state dynamics, transient absorption spectroscopy.

In vitro transcribed mRNAs have recently taken center stage in the field of medicinal therapeutics given their vital role in fighting the COVID-19 global pandemic.¹⁻³ The efficacy of these mRNA therapeutics is significantly increased by the use of non-canonical nucleobases within the sequence.⁴⁻⁷ The RNA derivatives pseudouridine, its N₁-methylated analogue, and 5-methylcytidine (5mCyd) have been identified to have the largest beneficial effect in medicinal

therapy. ^{4,5,8} Although these molecules were not selected to be one of the four building blocks of life, both pseudouridine and 5-methylcytidine are in fact naturally occurring and can form Watson-Crick base pairs. Furthermore, while 5mCyd has most commonly been identified as an epigenetic marker in DNA regulating expression of certain genes,⁹ this methylation of cytosine is also prevalent in RNA. Indeed, C₅-methylation of cytosine has recently been associated with a wide range of cellular functions including nuclear RNA export, mRNA translation, cell cycle control, cell differentiation / proliferation, and cancers. ^{10–15}

If 5mCyd is going to be purposefully incorporated into medical therapeutics, it is important to understand its chemical integrity and stability following light exposure and to evaluate its possible interaction with sunlight radiation. As such, 5mCyd has been investigated using quantum chemical calculations, time-resolved fluorescence, and time-resolved transient absorption techniques. 16-21 However, these studies have conflicting conclusions regarding the proposed electronic relaxation mechanism of 5mCyd. Work by Ma et al.¹⁶, Martínez-Fernández et al.,¹⁸ and Malone et al.²⁰ proposed that the major relaxation pathway of the $1\pi\pi^*$ state is the non-radiative decay of its population in approximately 7 ps, with no observation of long-lived excited state species. Conversely, recent work by Wang et al.¹⁹ observed the population of a long-lived excited state with a decay lifetime at least two to three orders of magnitude longer (> 8 ns). Because the likelihood of photoinduced damage increases as the excited state lifetime increases, it is important to resolve the contradictory results reported in the literature for 5mCyd. This is particularly important when 5mCyd is used in mRNA therapeutics, where unintended consequences of photoinitiated RNA damage could occur. In this Letter, steady-state and time-resolved absorption spectroscopy are combined with low-intensity laser irradiation experiments to investigate the excited state dynamics of 5-methylcytidine (5mCyd, Scheme 1) and its photodegradation rate and

relative photostability under equal experimental conditions compared to the canonical RNA nucleoside, cytidine (Cyd).

Scheme 1. Chemical structures of 5-methylcytidine (5mCyd, left) and cytidine (Cyd, right), where the R denotes the ribonucleoside.

Figure 1 shows the molar absorption and fluorescence emission spectra of 5mCyd and Cyd in phosphate buffer, pH 7.4. At this pH, both molecules are neutral tautomers with pKa values of 4.3 and 4.2 for 5mCyd²² and Cyd,²³ respectively. Upon methylation at the C₅-position, a red shift of approximately 7 nm is observed, thereby allowing for more absorption into the UVB region of the electromagnetic spectrum reaching the Earth's surface. The absorption spectrum of each molecule shows three band maxima at ca. 278, 239, and 213 nm for 5mCyd and at 271, 232, and < 200 nm for Cyd. This red shift is supported by previous steady-state experiments^{18,21,24,25} and quantum chemical calculations in water performed at the MS-CASPT2/MM level of theory.^{17,18} Molar absorption coefficients of 7,942 \pm 62 and 9,337 \pm 30 were obtained for 5mCyd and Cyd at 278 and 271 nm, respectively. A red shift is also observed in the fluorescence emission spectrum of 5mCyd compared to that of Cyd, with maxima at ca. 345 nm and 330 nm, respectively, following excitation at 255 nm (Figure 1b). Using thymidine as a standard,²⁶ a fluorescence quantum yield of 5.0 \times 10⁻⁴ was estimated for 5mCyd, which is about 5 \times larger than the quantum yield for Cyd of 1.0 \times

10⁻⁴. These fluorescence quantum yields and spectral shifts are in good agreement with those previously reported by Sharonov et al.²¹ and Martínez-Fernández et al.^{17,18} for the 2'-deoxyribose analogs (5mdCyd and dCyd). The excitation spectra taken at the emission maxima align well with the lowest energy absorption band of 5mCyd and Cyd, respectively, indicating that the emission is an intrinsic property of these nucleosides (Figure S1). Using the steady-state photophysical data and the Strickler-Berg equation,^{27,28} fluorescence lifetimes of 4.0 and 0.6 ps were estimated for 5mCyd and Cyd, respectively (see SI for details). These Strickler-Berg fluorescence lifetimes are in relatively good agreement with the experimentally obtained fluorescence lifetimes of 4.3 to 6.1^{18,21} for 5mdCyd and 0.720 ps²⁹ for Cyd.

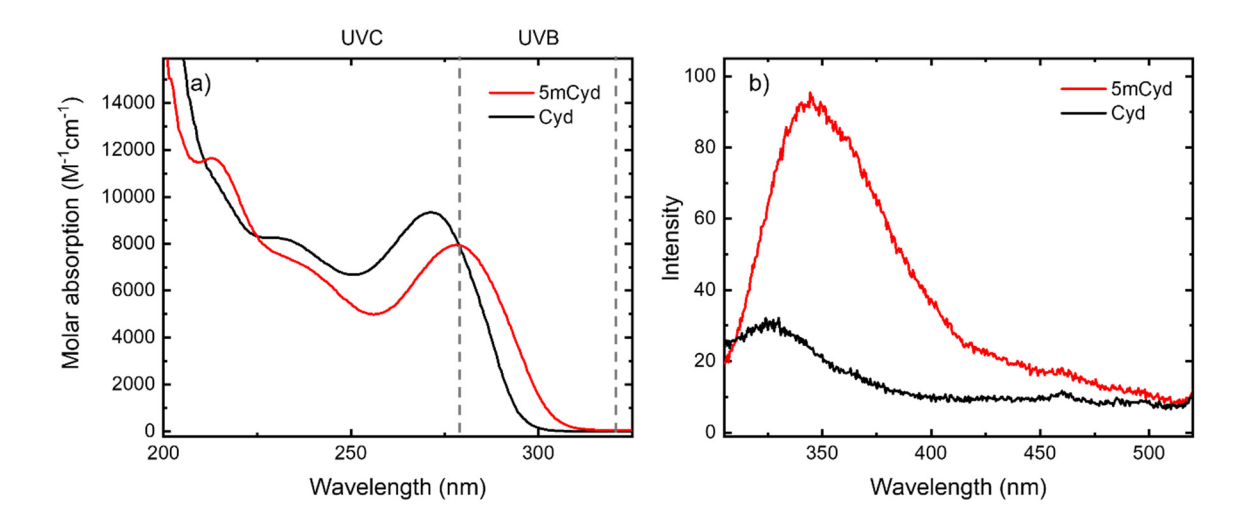


Figure 1. (a) Molar absorption spectra of 5mCyd (red) and Cyd (black) in 16 mM phosphate buffer, pH 7.4. (b) Steady-state fluorescence emission spectra of 5mCyd (red) and Cyd (black) following excitation at 255 nm using a PMT voltage of 800 V with 5 nm slit widths and a scan rate of 20 nm/min.

To investigate the electronic relaxation pathways of 5mCyd upon excitation at 267 nm, femtosecond broadband transient absorption spectroscopy was performed in back-to-back

experiments with the Cyd. As described in detail in the SI, the transient absorption data were corrected for the hydrated electron signal that originates from the two-photon absorption of the water solvent using the method developed by Kohler and coworkers.³⁰ Importantly, we also collected transient data exciting at 267 nm with low photon density conditions to avoid the formation of hydrated electrons from the solvent, as previously described.^{31–33} The latter results are shown in Figures S2 to S6. The transient absorption signals under both conditions are very similar from ca. 430 to 700 nm once the transient spectra under higher photon density conditions are corrected for the hydrated electron signal. However, as explained elsewhere³¹ and in the SI, the transient spectra in Figure 2 is overcorrected from ca. 320 to 450 nm due to an additional coherent signal from the solvent within the cross correlation of the pump and probe beams in this spectral region (see Figure S7).

Following excitation of 5mCyd at 267 nm, a broad transient species is observed with maxima below 320 and 550 nm and a negative amplitude ΔA signal that grows in at ca. 350 nm (Figure 2a). This negative amplitude ΔA signal corresponds very well with the steady-state fluorescence emission and therefore, is assigned to stimulated emission. During the time delays between 0.15 and 0.99 ps, a decrease and blue shift in amplitude in the UV region is observed with a maximum at ca. 360 nm, while a small red shift is observed in the visible region (Figure 2b). Finally, as shown in Figure 2c, a uniform decay across the entire probe region is observed between 0.99 and 31 ps. Similarly, for Cyd, a broad transient species is observed following excitation with maxima below 320 and at ca. 400 and 580 nm (Figure 2d,e). Between time delays of 0.13 and 3.2 ps, a decrease in the amplitude of the band at 580 nm is observed, while the band around 400 nm barely changes in amplitude (Figure 2e). From 3.2 to ca. 90 ps, the absorption bands with maxima below 320 and at ca. 400 nm fully decay and no other transient signal is observed at 2.7 ns (Figure 2f).

The full broadband transient absorption data for 5mCyd and Cyd were satisfactorily fitted with a two and three-component sequential kinetic model, respectively. The global, average lifetimes are reported in Table 1. Evolution associated difference spectra (EADS) and representative kinetic traces extracted from the global and target analyses of the solvent-corrected transient data are shown in Figure 3, while those under low photon density conditions are reported in Figures S3 and S4. We remark that the transient data that are corrected for the solvent signal (i.e., under high photon density) and the transient data that do not require solvent correction (i.e., under low photon density) can be satisfactorily globally fit with the same set of lifetimes shown in Table 1.

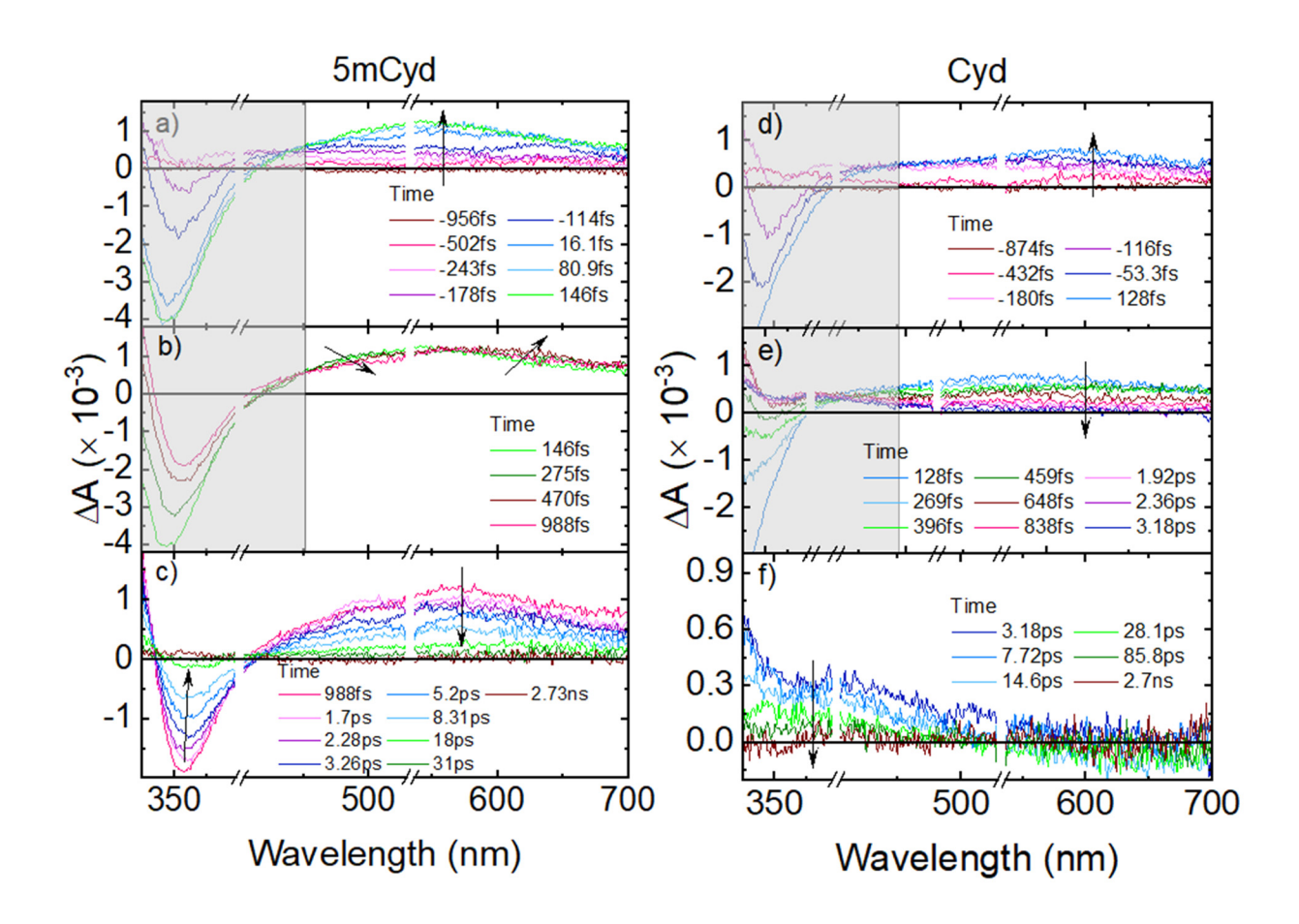


Figure 2. Selected transient absorption spectra of 5mCyd (a-c) and Cyd (d-f) in 16 mM phosphate buffer pH 7.4, following excitation at 267 nm. Note, the break in the abscissa to remove the overtone of the pump. The gray boxes denote areas of overcorrection of hydrated electron due to an additional coherent signal from the solvent within the cross correlation of the pump and probe beams in this spectral region (i.e., from time delays of ca. -0.4 to 0.4 ps. See, Figure S7 in SI).

Table 1. Global lifetimes of 5mCyd and Cyd following excitation at 267 nm in phosphate buffer 7.4. All errors are reported as twice the standard deviation.

	5mCyd	Cyd
$\overline{ au_1}$	$0.2 \pm 0.1 \text{ ps}$	$0.1 \pm 0.1 \text{ ps}$
$ au_2$	$7.1 \pm 0.2 \text{ ps}$	$1.4 \pm 0.1 \text{ ps}$
$ au_3$	-	$43.7 \pm 8.1 \text{ ps}$

Based on quantum chemical calculations computed at the MS-CASPT2/MM level of theory in water, 18 the S_1 and S_2 excited states are predicted to be of $\pi\pi^*$ character, whereas the S_3 excited state is of $n_N\pi^*$ character for both 5mCyd and Cyd. The two low lying $^1\pi\pi^*$ excited states in the Franck-Condon (FC) region were found to be at 4.19 and 4.79 eV for 5mCyd and at 4.46 and 4.79 eV for Cyd. Therefore, following excitation at 267 nm, it is expected that both the S_1 and S_2 excited states could be populated simultaneously. In such a case, internal conversion from the S_2 to S_1 excited state is proposed to occur ultrafast, i.e., < 100 fs, and therefore, may not be observed within our experimental time resolution of approximately 250 fs. Hence, we assigned the first, instrument response-limited lifetime of 0.1 and 0.2 ps of each molecule to a movement along the S_1 potential

energy surface away from the FC region toward a local minimum. This is supported by the computational work by Martínez-Fernández et al. 18 and Pepino et al. 34 The former group found minima for both 5mCyd and Cyd using TD-CAM-B3LYP/6-31(d) and MS-CASPT2(14,10)/ANO-L level of theory. The latter group also found the same two minima for Cyd, one planar and one bent minimum, and additionally a third minimum accessed after the S₂/S₁ conical intersection (CI), which has out-of-plane puckering at C₄ with strong coupling to the 1 n₀ π^* excited state.³⁴ The black EADS 1 in Figures 3b and S3 is therefore, assigned to a linear combination of the ${}^{1}\pi\pi^{*}$ planar, twist, and C₄ out-of-plane puckered minima, and possibly with some contribution from the ${}^{1}n_{N}\pi^{*}$ state, which is in good agreement with the simulated excited state absorption spectra (ESA) computed by Pepino et al.³⁴ The small fluorescence quantum yield of ca. 10^{-4} for both molecules, lend support to the idea that the S₁ minimum of both 5mCyd and Cyd is fairly shallow. For Cyd, we propose two primary relaxation pathways occur from the S₁ minimum: (1) fluorescence and (2) $S_1 \pi \pi^* \to S_0$ internal conversion. This competitive process is assigned to the second lifetime of 1.4 \pm 0.1 ps. The decay of the $^{1}\pi\pi^{*}$ via fluorescence and internal conversion is in good agreement with those reported previously for cytosine, where the conical intersection is accessed through out-of-plane ethylenic twisting of the C₅-C₆ bond. ^{16,20,35-42} The red EADS 2 (Figures 3b and S3b) is assigned to a combination of the $1\pi\pi^*$ twist and C₄ out of plane puckered minima. Lastly, the third lifetime of 43.7 ± 8.1 ps for Cyd is assigned to nonradiative decay of the 1 nn π^* state, which is also in good agreement with the lifetime previously reported in literature. $^{16,43-46}$ It has been suggested that in cytosine the 1 nn π^* state is accessed near the FC region, however, it is still unclear if internal conversion originates from the $S_1 \pi \pi^*$, $S_2 \pi \pi^*$, or from both states. 16,42 The blue EADS 3 (Figure 3b) is therefore primarily assigned to the absorption of the ${}^{1}n_{N}\pi^{*}$ minimum, which is supported by the ESA of the ${}^{1}n_{N}\pi^{*}$ minimum predicted

by Pepino et al.⁴² Quantum chemical calculations for cytosine and 1-methylcytosine that includes explicit water molecules have shown that the 1 no π^{*} state is significantly higher in energy and should not be populated upon excitation at 267 nm.⁴⁷ However, we cannot rule out unequivocally a small participation of the 1 no π^{*} state (see discussion in the SI). We remark that a triplet quantum yield of about 1% has been proposed for cytosine in aqueous solution.^{35,36} If such a small fraction of the population reaching the 1 nn π^{*} state in Cyd is indeed able to intersystem cross to the triplet sate, it is possible that we are unable to detect it within the sensitivity of the spectrometer. We note, however, that while decay channels involving intersystem crossing to the triplet manifold have been investigated computationally for Cyd,⁴² there is currently minimal experimental evidence^{35,36} and no computational evidence⁴⁷ supporting the population of the triplet state in Cyd in aqueous solution. Furthermore, the transient absorption experiments by Wang et al.¹⁹ and Ma et al.¹⁶ do not observe the population of a triplet state, in agreement with our results.

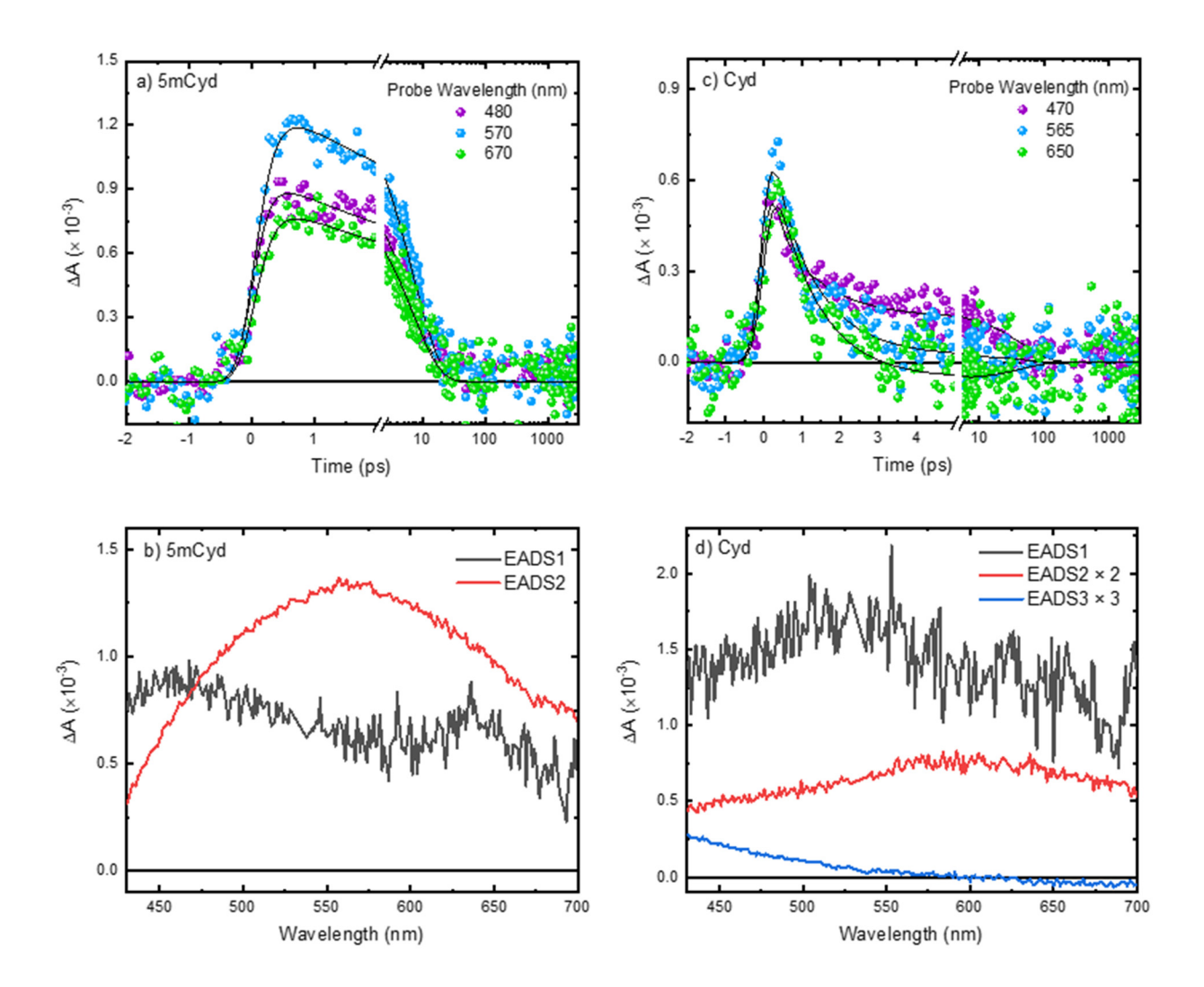


Figure 3. Representative kinetic traces and evolution associated difference spectra (EADS) of 5mCyd (a,b) and Cyd (c,d) following excitation at 267 nm in phosphate buffer pH 7.4, globally fit with a three or two-component sequential model, respectively. See Figure S3 in the SI, which reports the EADSs from ca. 320 to 700 nm. Note, in panel (c), EADS2 and EADS3 have been scaled by a factor of 2 and 5, respectively.

Following ultrafast $S_2 \rightarrow S_1$ internal conversion and movement along the S_1 potential energy surface, 5mCyd is proposed to decay primarily through nonradiative relaxation to the ground state,

with a small amount of the excited state population decaying via fluorescence. Similar to Cyd, the second lifetime is assigned to a competitive process between fluorescence (minor pathway) and S_1 $^1\pi\pi^* \to S_0$ internal conversion (primary pathway). Importantly, however, with a lifetime value of 7.1 \pm 0.2 ps, and consistent with the five-fold larger fluorescence yield of 5mCyd compared to Cyd, the decay lifetime of the $S_1\pi\pi^*$ state in 5mCyd is $5\times$ longer than that observed for Cyd, suggesting an energetic barrier might retard access to the S_1/S_0 ethylenic twisting CI. This idea is supported by quantum chemical calculations that demonstrated an energetic barrier of ca. 0.1 to 0.3 eV between the bent global minima and S_1/S_0 ethylenic twist CI of 5mCyd compared to an barrier of \leq 0.1 for Cyd. We also note that our reported S_1 lifetime for 5mCyd is in good agreement with that previously reported by Sharonov et al., 21 Ma et al., 16 Wang et al., 19 Martínez-Fernández et al., 18 and Malone et al. 20 using time resolved fluorescence and absorption spectroscopies.

Interestingly, the work by Wang et al. ¹⁹ also reported the population of a long-lived excited state in 5mCyd, preliminarily assigned to a 1 n π * state, persisting beyond a few nanoseconds in buffer solution at pH 7.4. This observation is in contrast to the transient absorption results reported in Figures 2 and S2, which show full decay of the excited state population within tens of picoseconds. We note that the results presented in Figures 2 and S2 are in agreement with those of Ma et al. ¹⁶ Since Wang et al. performed the correction of the two-photon ionization solvent signal, ³⁰ it is currently unclear why they observed a long-lived nanosecond signal with absorption maximum around 670 nm but we and others ¹⁶ do not. Unfortunately, we cannot rule out the possibility of an impurity contributing to their transient data because the authors did not reported the emission and excitation spectra of the solutions. ¹⁹ We remark, however, that all other transient absorption results reported in this Letter, and by Ma et al., ¹⁶ are consistent with those reported by Wang et al. ¹⁹

To investigate the photoreactivity of 5mCyd relative to Cyd, low intensity laser irradiation experiments were performed back-to-back exciting at 267 nm with a matched absorbance at the excitation wavelength (Figure 4), as has been reported recently for N1-methylpseudouridine and uridine.³³ Irradiation of both molecules results in a decrease in absorbance at the lowest energy band and at the higher energy absorption band near 200 nm. A simultaneous increase in absorbance and red shift is observed for the absorption band originally at 239 and 232 nm for 5mCyd and Cyd, respectively. In addition, isosbestic points are observed at 228 and 252 nm for Cyd. These changes in the absorption spectra with an increased irradiation time evidence the formation of photoproducts for both 5mCyd and Cyd. We note that similar absorption trends were detected by Todd et al.⁴⁸ and Burr et al.⁴⁹ for Cyd. Importantly, however, we demonstrate that 5mCyd photodegrades with a rate that is three-fold smaller than Cyd under identical experimental conditions at pH of 7.4. The increased photostability of 5mCyd compared to Cyd is also consistent with the population of an excited state in Cyd that is six-fold longer-lived than the longest excited state in 5mCyd (Figure 2 and Table 1).

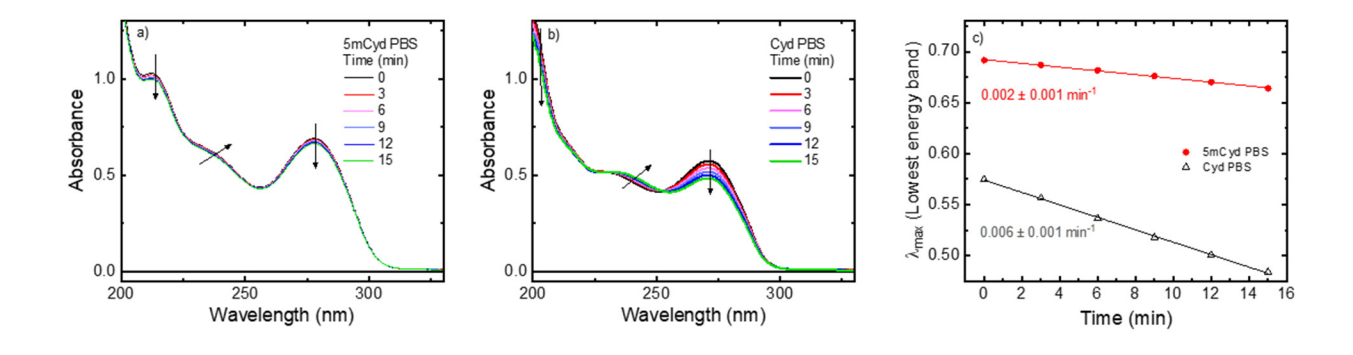


Figure 4. Photodegradation of 5mCyd (a) and Cyd (b) following low intensity laser irradiation at 267 nm in back-to-back experiments with matched optical densities at excitation wavelength in 16 mM phosphate buffer pH 7.4, under ambient conditions. Initial rates of photodegradation for Cyd

(black triangles) and 5mCyd (red circles) are shown in panel c. Errors are reported as twice the standard deviation.

Before closing, we present high-performance liquid chromatography (HPLC) and computational results, and photodegradation experiments in acetonitrile, in the SI to partially characterize the primary photoproducts formed in both 5mCyd and Cyd under the experimental conditions used in this work (see Figures S8 to S13). We remark that the complete characterization and identification of the Cyd photoproducts have proven challenging because of the formation of photohydrates is reversible and the possibility of deamination at the C₄ position.^{49,50} The report of a longer-lived 1 n π^* state in this Letter, and in previous works, $^{16,43-46}$ which is not detected in 5mCyd (Figure 2), lend important support to the idea that a 1 n π^* excited state of Cyd participates in the formation of one or more of these photoproducts.⁴⁷ This seems to be particularly the case for the 6-hydroxycytidine photohydrate (see Figure S10 and discussion in the SI).

Through the combination of steady state absorption/emission, time resolved absorption spectroscopy, and low-intensity laser irradiation experiments, we have investigated the excited state relaxation pathways for both 5mCyd and Cyd upon excitation at 267 nm and reported a three-fold higher relative photostability of 5mCyd compared to the canonical RNA nucleoside Cyd in phosphate buffer pH 7.4. We have also shown that a ${}^{1}n\pi^{*}$ state of Cyd decays with a lifetime of ca. 44 ps in aqueous solution upon excitation at 267 nm and detected no spectroscopic evidence for the population of a nanosecond excited state. The ${}^{1}n\pi^{*}$ state is directly implicated in the formation of 6-hydroxycytidine and other primary photoproducts. The slower S₁ $\pi\pi^{*}$ state internal conversion to the ground state observed in 5mCyd compared to Cyd, is proposed to be due to the higher energy barrier required to access the ethylenic C₅-C₆ twist S₁/S₀ conical intersection due to the presence of the methyl group. We highlight that even though the ${}^{1}\pi\pi^{*}$ excited state decay is 5-

fold slower in 5mCyd than in Cyd, the three-fold decreased photodegradation rate demonstrates that monomeric 5mCyd is more photostable than Cyd in aqueous solution at pH 7.4 and suggests that a 1 n π^* state plays an important role in the formation of photoproducts in Cyd, as previously proposed. Given that the primary photoproducts observed in 5mCyd have similar absorption spectra than those of Cyd (see Figure S9 in the SI), it is possible that an analogous 1 n π^* state is also populated in 5mCyd but at ca. three-fold lower yield than in Cyd. This idea, together with the fact that stimulated emission in 5mCyd occurs in the same spectral region, could explain why a 1 n π^* state is not detected in Figures 2, S2, and S5. Finally, the three-fold lower photodegradation of 5mCyd compared to Cyd suggests that 5mCyd could be a safe choice for incorporation into mRNA vaccines. However, we remark that future research to investigate the photoreactivity of 5mCyd when incorporated in single and double-stranded RNA oligonucleotides is essential because base stacking and base pairing interactions, and its different redox potential compared to Cyd, could significantly change its photostability when incorporate into RNA.

ASSOCIATED CONTENT

Supporting Information. Experimental and computational methodology, supporting discussion including excitation spectra, transient absorption and photodegradation data under low photon density conditions, photodegradation experiments for 5mCyd and Cyd in dry (< 0.01% water) acetonitrile, HPLC separation of the primary photoproducts, experimental and calculated absorption spectra of the primary photoproducts, and neat phosphate buffer transient absorption spectra under both high and low photon density conditions.

AUTHOR INFORMATION

Sean J. Hoehn: conceptualization, investigation, formal analysis, writing-original draft, writing review and editing.

Sarah E. Krul: investigation, formal analysis, writing-original draft, writing review and editing. Michael Pogharian: formal analysis, writing review.

Ergian Mao: investigation and editing.

Carlos E. Crespo-Hernández: conceptualization, funding acquisition, project administration, resources, supervision, visualization, validation, writing review and editing.

Notes

The authors declare no conflicts of interest.

ACKNOWLEDGMENT

The authors acknowledge funding from the National Science Foundation (Grant No. CHE-1800052) and the High-Performance Computing Resource in the Core Facility for Advanced Research Computing at Case Western Reserve University. The authors also thank Dr. Shane Parker for providing computational resources to perform the calculations reported in this study.

References

- (1) Nance, K. D.; Meier, J. L. Modifications in an Emergency: The Role of N1-Methylpseudouridine in COVID-19 Vaccines. *ACS Cent. Sci.* **2021**, 7 (5), 748–756. https://doi.org/10.1021/acscentsci.1c00197.
- (2) May, M. After COVID-19 Successes, Researchers Push to Develop MRNA Vaccines for Other Diseases. *Nat. Med.* 2021, 27 (6), 930–932. https://doi.org/10.1038/s41591-021-01393-8.

- (3) Verbeke, R.; Lentacker, I.; De Smedt, S. C.; Dewitte, H. The Dawn of MRNA Vaccines: The COVID-19 Case. *J. Control. Release* **2021**, *333* (February), 511–520. https://doi.org/10.1016/j.jconrel.2021.03.043.
- (4) Karikó, K.; Muramatsu, H.; Welsh, F. A.; Ludwig, J.; Kato, H.; Akira, S.; Weissman, D. Incorporation of Pseudouridine into MRNA Yields Superior Nonimmunogenic Vector with Increased Translational Capacity and Biological Stability. *Mol. Ther.* 2008, *16* (11), 1833–1840. https://doi.org/10.1038/mt.2008.200.
- (5) Karikó, K.; Buckstein, M.; Ni, H.; Weissman, D. Suppression of RNA Recognition by Toll-like Receptors: The Impact of Nucleoside Modification and the Evolutionary Origin of RNA. *Immunity* **2005**, *23* (2), 165–175. https://doi.org/10.1016/j.immuni.2005.06.008.
- (6) Kim, S. C.; Sekhon, S. S.; Shin, W. R.; Ahn, G.; Cho, B. K.; Ahn, J. Y.; Kim, Y. H. Modifications of MRNA Vaccine Structural Elements for Improving MRNA Stability and Translation Efficiency. *Mol. Cell. Toxicol.* 2022, 18 (1), 1–8. https://doi.org/10.1007/s13273-021-00171-4.
- (7) Laczkó, D.; Hogan, M. J.; Toulmin, S. A.; Hicks, P.; Lederer, K.; Gaudette, B. T.; Castaño, D.; Amanat, F.; Muramatsu, H.; Oguin, T. H.; Ojha, A.; Zhang, L.; Mu, Z.; Parks, R.; Manzoni, T. B.; Roper, B.; Strohmeier, S.; Tombácz, I.; Arwood, L.; Nachbagauer, R.; Karikó, K.; Greenhouse, J.; Pessaint, L.; Porto, M.; Putman-Taylor, T.; Strasbaugh, A.; Campbell, T. A.; Lin, P. J. C.; Tam, Y. K.; Sempowski, G. D.; Farzan, M.; Choe, H.; Saunders, K. O.; Haynes, B. F.; Andersen, H.; Eisenlohr, L. C.; Weissman, D.; Krammer, F.; Bates, P.; Allman, D.; Locci, M.; Pardi, N. A Single Immunization with Nucleoside-Modified MRNA Vaccines Elicits Strong Cellular and Humoral Immune Responses against

- SARS-CoV-2 in Mice. *Immunity* **2020**, *53* (4), 724-732.e7. https://doi.org/10.1016/j.immuni.2020.07.019.
- (8) Andries, O.; Mc Cafferty, S.; De Smedt, S. C.; Weiss, R.; Sanders, N. N.; Kitada, T. N1-Methylpseudouridine-Incorporated MRNA Outperforms Pseudouridine-Incorporated MRNA by Providing Enhanced Protein Expression and Reduced Immunogenicity in Mammalian Cell Lines and Mice. *J. Control. Release* 2015, 217, 337–344. https://doi.org/10.1016/j.jconrel.2015.08.051.
- (9) Kumar, S.; Chinnusamy, V.; Mohapatra, T. Epigenetics of Modified DNA Bases: 5-Methylcytosine and Beyond. *Front. Genet.* **2018**, *9* (December), 1–14. https://doi.org/10.3389/fgene.2018.00640.
- (10) Li, Q.; Li, X.; Tang, H.; Jiang, B.; Dou, Y.; Gorospe, M.; Wang, W. NSUN2-Mediated M5C Methylation and METTL3/METTL14-Mediated M6A Methylation Cooperatively Enhance P21 Translation. J. Cell. Biochem. 2017, 118 (9), 2587–2598. https://doi.org/10.1002/jcb.25957.
- (11) Liu, J.; Jia, G. Methylation Modifications in Eukaryotic Messenger RNA. *J. Genet. Genomics* **2014**, *41* (1), 21–33. https://doi.org/10.1016/j.jgg.2013.10.002.
- (12) Frye, M.; Harada, B. T.; Behm, M.; He, C. RNA Modifications Modulate Gene Expression during Development. *Science* **2018**, *361* (6409), 1346–1349. https://doi.org/10.1126/science.aau1646.
- (13) Yang, X.; Yang, Y.; Sun, B. F.; Chen, Y. S.; Xu, J. W.; Lai, W. Y.; Li, A.; Wang, X.; Bhattarai, D. P.; Xiao, W.; Sun, H. Y.; Zhu, Q.; Ma, H. L.; Adhikari, S.; Sun, M.; Hao, Y.

- J.; Zhang, B.; Huang, C. M.; Huang, N.; Jiang, G. Bin; Zhao, Y. L.; Wang, H. L.; Sun, Y. P.; Yang, Y. G. 5-Methylcytosine Promotes MRNA Export-NSUN2 as the Methyltransferase and ALYREF as an m 5 C Reader. *Cell Res.* **2017**, *27* (5), 606–625. https://doi.org/10.1038/cr.2017.55.
- (14) Frye, M.; Watt, F. M. The RNA Methyltransferase Misu (NSun2) Mediates Myc-Induced Proliferation and Is Upregulated in Tumors. *Curr. Biol.* **2006**, *16* (10), 971–981. https://doi.org/10.1016/j.cub.2006.04.027.
- (15) Blaze, J.; Navickas, A.; Phillips, H. L.; Heissel, S.; Plaza-Jennings, A.; Miglani, S.; Asgharian, H.; Foo, M.; Katanski, C. D.; Watkins, C. P.; Pennington, Z. T.; Javidfar, B.; Espeso-Gil, S.; Rostandy, B.; Alwaseem, H.; Hahn, C. G.; Molina, H.; Cai, D. J.; Pan, T.; Yao, W. D.; Goodarzi, H.; Haghighi, F.; Akbarian, S. Neuronal Nsun2 Deficiency Produces TRNA Epitranscriptomic Alterations and Proteomic Shifts Impacting Synaptic Signaling and Behavior. *Nat. Commun.* 2021, 12 (1), 1–16. https://doi.org/10.1038/s41467-021-24969-x.
- (16) Ma, C.; Cheng, C. C.-W.; Chan, C. T.-L.; Chan, R. C.-T.; Kwok, W.-M. Remarkable Effects of Solvent and Substitution on the Photo-Dynamics of Cytosine: A Femtosecond Broadband Time-Resolved Fluorescence and Transient Absorption Study. *Phys. Chem. Chem. Phys.* 2015, 17 (29), 19045–19057. https://doi.org/10.1039/C5CP02624E.
- (17) Martínez-Fernández, L.; Pepino, A. J.; Segarra-Martí, J.; Banyasz, A.; Garavelli, M.; Improta, R. Computing the Absorption and Emission Spectra of 5-Methylcytidine in Different Solvents: A Test-Case for Different Solvation Models. *J. Chem. Theory Comput.*2016, 12 (9), 4430–4439. https://doi.org/10.1021/acs.jctc.6b00518.

- (18) Martínez-Fernández, L.; Pepino, A. J.; Segarra-Martí, J.; Jovaišaitei, J.; Vaya, I.; Nenov, A.; Markovitsi, D.; Gustavsson, T.; Banyasz, A.; Garavelli, M.; Improta, R. Photophysics of Deoxycytidine and 5-Methyldeoxycytidine in Solution: A Comprehensive Picture by Quantum Mechanical Calculations and Femtosecond Fluorescence Spectroscopy. *J. Am. Chem. Soc.* 2017, 139 (23), 7780–7791. https://doi.org/10.1021/jacs.7b01145.
- (19) Wang, X.; Zhou, Z.; Tang, Y.; Chen, J.; Zhong, D.; Xu, J. Excited State Decay Pathways of 2'-Deoxy-5-Methylcytidine and Deoxycytidine Revisited in Solution: A Comprehensive Kinetic Study by Femtosecond Transient Absorption. *J. Phys. Chem. B* **2018**, *122* (28), 7027–7037. https://doi.org/10.1021/acs.jpcb.8b00927.
- (20) Malone, R. J.; Miller, A. M.; Kohler, B. Singlet Excited-State Lifetimes of Cytosine Derivatives Measured by Femtosecond Transient Absorption. *Photochem. Photobiol.* 2003, 77 (2), 158–164. https://doi.org/10.1562/0031-8655(2003)077<0158:SESLOC>2.0.CO;2.
- (21) Sharonov, A.; Gustavsson, T.; Marguet, S.; Markovitsi, D. Photophysical Properties of 5-Methylcytidine. *Photochem. Photobiol. Sci.* **2003**, *2* (4), 362–364. https://doi.org/10.1039/b212664h.
- (22) Fox, J. J.; Van Praag, D.; Wempen, I.; Doerr, I. L.; Cheong, L.; Knoll, J. E.; Eidinoff, M. L.; Bendich, A.; Brown, G. B. Thiation of Nucleosides. II. Synthesis of 5-Methyl-2'-Deoxycytidine and Related Pyrimidine Nucleosides 1. *J. Am. Chem. Soc.* 1959, 81 (1), 178–187. https://doi.org/10.1021/ja01510a042.
- (23) Shugar, D.; Fox, J. J. Spectrophotometric Studies Op Nucleic Acid Derivatives and Related Compounds as a Function of PH. *Biochim. Biophys. Acta* **1952**, *9*, 199–218. https://doi.org/10.1016/0006-3002(52)90147-9.

- (24) Basanta-Sanchez, M.; Temple, S.; Ansari, S. A.; D'Amico, A.; Agris, P. F. Attomole Quantification and Global Profile of RNA Modifications: Epitranscriptome of Human Neural Stem Cells. *Nucleic Acids Res.* **2016**, *44* (3), e26–e26. https://doi.org/10.1093/nar/gkv971.
- (25) Ai, Y.; Xing, J.; Zhang, A.; Zhao, C.; Liu, Y.; Xie, B.; Chen, W.; Cui, G.; Lu, Z.; Wang, X. Computational Study on the Excited-State Decay of 5-Methylcytosine and 5-Hydroxymethylcytosine: The Common Form of DNA Methylation and Its Oxidation Product. *J. Phys. Chem. B* **2018**, *122* (46), 10424–10434. https://doi.org/10.1021/acs.jpcb.8b07830.
- (26) Onidas, D.; Markovitsi, D.; Marguet, S.; Sharonov, A.; Gustavsson, T. Fluorescence Properties of DNA Nucleosides and Nucleotides: A Refined Steady-State and Femtosecond Investigation. J. Phys. Chem. B 2002, 106 (43), 11367–11374. https://doi.org/10.1021/jp026063g.
- (27) Cohen, B.; Crespo-Hernández, C. E.; Kohler, B. Strickler–Berg Analysis of Excited Singlet State Dynamics in DNA and RNA Nucleosides. *Faraday Discuss.* **2004**, *127*, 137–147. https://doi.org/10.1039/B316939A.
- (28) Strickler, S. J.; Berg, R. A. Relationship between Absorption Intensity and Fluorescence Lifetime of Molecules. *J. Chem. Phys.* **1962**, *37* (4), 814–822. https://doi.org/10.1063/1.1733166.
- (29) Pecourt, J. M. L.; Peon, J.; Kohler, B. DNA Excited-State Dynamics: Ultrafast Internal Conversion and Vibrational Cooling in a Series of Nucleosides. *J. Am. Chem. Soc.* **2001**, *123* (42), 10370–10378. https://doi.org/10.1021/ja0161453.

- (30) Crespo-Hernández, C. E.; Kohler, B. Influence of Secondary Structure on Electronic Energy Relaxation in Adenine Homopolymers. *J. Phys. Chem. B* **2004**, *108* (30), 11182–11188. https://doi.org/10.1021/jp0496046.
- (31) Krul, S. E.; Hoehn, S. J.; Feierabend, K. J.; Crespo-Hernández, C. E. Excited State Dynamics of 7-Deazaguanosine and Guanosine 5'-Monophosphate. *J. Chem. Phys.* **2021**, 154 (7), 075103. https://doi.org/10.1063/5.0038123.
- (32) Krul, S. E.; Costa, G. J.; Hoehn, S. J.; Valverde, D.; Oliveira, L. M. F.; Borin, A. C.; Crespo-Hernández, C. E. Resolving Ultrafast Photoinitiated Dynamics of the Hachimoji 5-aza-7deazaguanine Nucleobase: Impact of Synthetically Expanding the Genetic Alphabet. *Photochem. Photobiol.* **2023**, *99* (2), 693–705. https://doi.org/10.1111/php.13688.
- (33) Hoehn, S. J.; Krul, S. E.; Skory, B. J.; Crespo-Hernández, C. E. Increased Photostability of the Integral mRNA Vaccine Component N1-Methylpseudouridine Compared to Uridine. *Chem. A Eur. J.* **2022**, *28* (6), e202103667. https://doi.org/10.1002/chem.202103667.
- (34) Pepino, A. J.; Segarra-Martí, J.; Nenov, A.; Improta, R.; Garavelli, M. Resolving Ultrafast Photoinduced Deactivations in Water-Solvated Pyrimidine Nucleosides. *J. Phys. Chem. Lett.* **2017**, *8* (8), 1777–1783. https://doi.org/10.1021/acs.jpclett.7b00316.
- (35) Hare, P. M.; Crespo-Hernández, C. E.; Kohler, B. Internal Conversion to the Electronic Ground State Occurs via Two Distinct Pathways for Pyrimidine Bases in Aqueous Solution. *Proc. Natl. Acad. Sci.* **2007**, *104* (2), 435–440. https://doi.org/10.1073/pnas.0608055104.
- (36) Nikogosyan, D. N.; Angelov, D. A.; Oraevsky, A. A. Determination of Parameters of Excited States of DNA and RNA Bases by Laser UV Photolysis. *Photochem. Photobiol.*

- **1982**, 35 (5), 627–635. https://doi.org/10.1111/j.1751-1097.1982.tb02621.x.
- (37) Kistler, K. A.; Matsika, S. Three-State Conical Intersections in Cytosine and Pyrimidinone Bases. *J. Chem. Phys.* **2008**, *128* (21), 215102. https://doi.org/10.1063/1.2932102.
- (38) Kistler, K. A.; Matsika, S. Cytosine in Context: A Theoretical Study of Substituent Effects on the Excitation Energies of 2-Pyrimidinone Derivatives. *J. Phys. Chem. A* **2007**, *111* (35), 8708–8716. https://doi.org/10.1021/jp074361d.
- (39) Serrano-Andrés, L.; Merchán, M. Are the Five Natural DNA/RNA Base Monomers a Good Choice from Natural Selection?. A Photochemical Perspective. *J. Photochem. Photobiol. C Photochem. Rev.* **2009**, *10* (1), 21–32. https://doi.org/10.1016/j.jphotochemrev.2008.12.001.
- (40) Merchán, M.; González-Luque, R.; Climent, T.; Serrano-Andrés, L.; Rodríguez, E.; Reguero, M.; Peláez, D. Unified Model for the Ultrafast Decay of Pyrimidine Nucleobases.
 J. Phys. Chem. B 2006, 110 (51), 26471–26476. https://doi.org/10.1021/jp066874a.
- (41) Merchán, M.; Serrano-Andrés, L. Ultrafast Internal Conversion of Excited Cytosine via the Lowest ππ* Electronic Singlet State. J. Am. Chem. Soc. 2003, 125 (27), 8108–8109. https://doi.org/10.1021/ja0351600.
- (42) Pepino, A. J.; Segarra-Martí, J.; Nenov, A.; Rivalta, I.; Improta, R.; Garavelli, M. UV-Induced Long-Lived Decays in Solvated Pyrimidine Nucleosides Resolved at the MS-CASPT2/MM Level. *Phys. Chem. Chem. Phys.* 2018, 20 (10), 6877–6890. https://doi.org/10.1039/C7CP08235E.
- (43) Barbatti, M.; Aquino, A. J. A.; Szymczak, J. J.; Nachtigallová, D.; Hobza, P.; Lischka, H.

- Relaxation Mechanisms of UV-Photoexcited DNA and RNA Nucleobases. *Proc. Natl. Acad. Sci.* **2010**, *107* (50), 21453–21458. https://doi.org/10.1073/pnas.1014982107.
- (44) Keane, P. M.; Wojdyla, M.; Doorley, G. W.; Watson, G. W.; Clark, I. P.; Greetham, G. M.; Parker, A. W.; Towrie, M.; Kelly, J. M.; Quinn, S. J. A Comparative Picosecond Transient Infrared Study of 1-Methylcytosine and 5'-dCMP That Sheds Further Light on the Excited States of Cytosine Derivatives. *J. Am. Chem. Soc.* 2011, 133 (12), 4212–4215. https://doi.org/10.1021/ja1106089.
- (45) Quinn, S.; Doorley, G. W.; Watson, G. W.; Cowan, A. J.; George, M. W.; Parker, A. W.; Ronayne, K. L.; Towrie, M.; Kelly, J. M. Ultrafast IR Spectroscopy of the Short-Lived Transients Formed by UV Excitation of Cytosine Derivatives. *Chem. Commun.* 2007, No. 21, 2130–2132. https://doi.org/10.1039/b703344c.
- (46) Miura, Y.; Yamamoto, Y. I.; Karashima, S.; Orimo, N.; Hara, A.; Fukuoka, K.; Ishiyama, T.; Suzuki, T. Formation of Long-Lived Dark States during Electronic Relaxation of Pyrimidine Nucleobases Studied Using Extreme Ultraviolet Time-Resolved Photoelectron Spectroscopy. *J. Am. Chem. Soc.* 2023, 145 (6), 3369–3381. https://doi.org/10.1021/jacs.2c09803.
- (47) Szabla, R.; Kruse, H.; Šponer, J.; Góra, R. W. Water-Chromophore Electron Transfer Determines the Photochemistry of Cytosine and Cytidine. *Phys. Chem. Chem. Phys.* **2017**, 19 (27), 17531–17537. https://doi.org/10.1039/c7cp02635h.
- (48) Todd, Z. R.; Fahrenbach, A. C.; Ranjan, S.; Magnani, C. J.; Szostak, J. W.; Sasselov, Di. D. Ultraviolet-Driven Deamination of Cytidine Ribonucleotides Under Planetary Conditions.
 Astrobiology 2020, 20 (7), 878–888. https://doi.org/10.1089/ast.2019.2182.

- (49) Burr, J. G. Nucleic Acid Derivatives. In *Thin-Layer Chromatography, Revised And Expanded*; CRC Press, 1999; Vol. 6, pp 212–217. https://doi.org/10.1201/9780203910214.ch20.
- (50) Fisher, G. J.; Johns, H. E. Pyrimidine Photohydrates. In *Photochemistry and Photobiology* of Nucleic Acids; Wang, S. Y., Ed.; Academic Press, 1976; pp 169–224. https://doi.org/https://doi.org/10.1016/B978-0-12-734601-4.50010-0.
- (51) Burr, J. G.; Park, E. H.; Chan, A. Nature of the Reactive Species in the Photohydration of Uracil and Cytosine Derivatives. *J. Am. Chem. Soc.* **1972**, *94* (16), 5866–5872. https://doi.org/10.1021/ja00771a054.

Photochemical Stability of 5-Methylcytidine Relative to Cytidine:

Photophysical Insight for mRNA Therapeutic Applications

Sean J. Hoehn, Sarah E. Krul, Michael M. Pogharian, Ergian Mao, Carlos E. Crespo-Hernández*

Department of Chemistry Case Western Reserve University 44106 Cleveland, Ohio (United States)

Supplemental Information

1. Materials and Methods

Cytidine (Cyd, 99% purity), 5-methylcytidine (5mCyd, > 99%), and extra dry acetonitrile (ACN) were purchased from Sigma Aldrich used as received. Phosphate buffer solutions with total phosphate concentration of 16 mM from monosodium and disodium phosphate salts dissociated in ultrapure water (Millipore) were freshly prepared the day of each laser irradiation experiment. The pH of the solution was adjusted using 0.1 M solutions of NaOH and HCl to the desired pH of 7.4 (\pm 0.1 pH units).

1.1 Steady-state Spectroscopy

Steady-state absorption and emission spectra were recorded using a Cary 100 and Cary Eclipse spectrometer, respectively. Excitation and emission spectra were obtained using a PMT voltage of 800 V with 5 nm slit widths and a scan rate of 20 nm/min. Solutions for emission and excitation spectra were prepared with an optical density of ~0.18 at excitation wavelengths of 255, and 267 nm (Figures S1 and S2). The fluorescence spectra were corrected for Raman emission of the solvent and for the lamp intensity at each respective wavelength. The fluorescence quantum yield was calculated following equation 1:

$$\Phi = \Phi_R \cdot \frac{I}{I_R} \cdot \frac{OD_R}{OD} \cdot \frac{n^2}{n_R^2}$$
 (1)

where Φ represents the fluorescence quantum yield, I is the integrated area under the emission spectrum, OD is the optical density at excitation wavelength, and n is the refractive index of the respective solvent. The subscript R denotes the fluorescence standard, thymidine, of known quantum yield.

1.2 Strickler-Berg Lifetimes

Fluorescence lifetimes were estimated using the Strickler-Berg (SB) equation (2) as previously described.^{3,4} Briefly, the steady-state absorption spectra measured in 16 mM phosphate buffer, pH 7.4 were plotted versus wavenumber. The area under the lower energy absorption band was integrated from 39290-31013 cm⁻¹ for 5mCyd and 39908-32265 cm⁻¹ for Cyd.

$$(\tau_0^{SB})^{-1} = \frac{1}{N_A} 8\pi n^2 [2303\langle \tilde{v}_f^{-3} \rangle^{-1}] \int \frac{\varepsilon(\tilde{v})}{\tilde{v}} d\tilde{v}$$
 (2)

In equation 2, n is the refractive index of the solvent, c is the speed of light, N_A is Avogadro's number, and \tilde{v}_f is the emission frequency in wavenumbers. $\langle \tilde{v}_f^{-3} \rangle^{-1}$ was estimated by the cube of the emission maximum of each nucleoside, 345 and 330 nm for 5mCyd and Cyd, respectively, in units of wavenumber. Lastly, fluorescence lifetime was estimated by multiplying the Strickler Berg radiative lifetime, τ_0^{SB} , by the experimentally obtained fluorescence quantum yield.

1.3 Low Intensity Irradiation Experiments

The degradation excitation laser source of 267 nm was generated from the 800 nm fundamental beam, as previously described by Krul et al. The excitation pulse was reduced to a spot size of ~3.0 mm (3.010 \pm 0.005 mm) using the knife edge method; while the average energy of the excitation beam was attenuated to 2 μJ with use of a neutral density filter, for an estimated average quantum flux of 3.8×10^{16} cm $^{-2}$ s $^{-1}$, as described in more detail elsewhere. The samples were matched at 0.65 absorbance units in 1 cm cuvettes at excitation wavelength for all solvents. The homogeneity of the solutions was maintained throughout the experiment through use of a Teflon-coated magnetic stir bar and a magnetic stir plate set to 1400 rpm.

1.4 Transient Absorption Spectroscopy

The experimental setup and data analysis used for the femtosecond broadband transient absorption spectroscopy (TAS) technique have been described in great deal elsewhere. Briefly, the TAS spectrometer (Helios, Ultrafast Systems) make use of a Ti:Sapphire oscillator (Vitesse, Coherent), which seeds a regenerative amplifier (Libra-HE, Coherent) producing 100 fs pulses, centered at 800 nm, and with a 1 kHz repetition rate. Generation of the 267 nm excitation pulse was done as described previously³³ by pumping an optical rail kit (FKE series, EKSMA optics). A translating 2 mm CaF₂ window was used to generate the white light continuum in the spectral probe window from 320 to 700 nm.

The absorbance of the sample solutions at the excitation wavelength were all matched at 1.1 and 1.65 during low intensity (average quantum flux of 1.7×10^{17} cm⁻² s⁻¹) and high intensity (average quantum flux of 8.6×10^{17} cm⁻² s⁻¹) TAS experiments, respectively. The homogeneity of the solutions in a 2 mm path length fused silica cell, was maintained by continuous stirring with a Teflon-coated magnetic stirbar. To minimize the putative contamination of the transient signals by the formation of any photoproducts absorbing at the excitation wavelengths, freshly prepared samples were used, and frequently refreshed over the course of data acquisition such that the absorption maximum of the samples at excitation wavelength did not decrease by more than 5 percent.

Data collection was performed with the Helios collection software, data pre-processing in Surface Explorer, while global and target data analyses were performed using the Glotaran graphical user interface to the R-package TIMP software. The full multidimensional data set for low intensity TAS experiments for Cyd was globally fit using a three component sequential kinetic model, whereas a two component sequential kinetic model was used for 5mCyd. The high intensity transient absorption data was cropped from 430-700 nm and then globally fit using the same kinetic modeling from the low intensity TAS. All kinetic fits were convoluted with a Gaussian instrument response function of 250 ± 50 fs (FWHM). The evolution associated difference spectra (EADS) were extracted from the global and target analysis.

1.5 Reverse Phase HPLC Separation

Samples were freshly prepared the day of each experiment in ultrapure water, pH 5.6, to have an absorbance of 1.0 at the excitation wavelength of 267 nm. Following one photon irradiation as described in the transient absorption spectroscopy methods, irradiated samples were analyzed by using a HPLC (Shimadzu LC-20AD) associated with a photodiode array (PDA) detector (Shimadzu SPD-M20A) at room temperature. A Synergi Fusion RP column (Phenomenex, 4 μ m, 25 cm \times 4.6 mm) was used to separate the parent chromophore from its photoproducts. A 10 μ L aliquot of the irradiated solution was injected into the HPLC through a manual injector. Ultrapure water (pH 5.6) was used to elute the sample with a flow rate of 0.5 mL min⁻¹.

1.6 Quantum Chemical Calculations

All calculations were performed using the ORCA¹² 5.0.2 software package. Ground state structures were optimized using the Gaussian electronic structure program implementation of the B3LYP (B3LYP_G)^{13,14} functional and excited state computations used the PBE0¹⁵ functional, all utilizing the def2-TZVPD basis set^{16,17} and D3BJ atom-pairwise dispersion correction to the DFT energy with Becke-Johnson damping. 18,19 All structures were optimized without any geometrical or symmetry constraints and were verified as true minima on the potential energy surface via frequency analysis, ensuring the Hessian matrix of energy second derivatives were without imaginary eigenvalues at the same level of theory. As previously described elsewhere, ²⁰ accelerating two electron integral computations, the resolution of the identity²¹ (RIJ) approximation was used for the Coulomb portion, while the chain of spheres exchange²² (COSX) algorithm was used for the exchange part of the electron-electron interaction. For ground state optimizations, the RIJCOSX approximation was turned off for the last steps of optimization. To model solvation in aqueous solution, all calculations took advantage of the default LR-CPCM model as well as the Gaussian charge scheme, where the number of Lebedev points were increased to 302. Additionally, calculations for the 6-OH photohydrate of cytosine, 6-hydroxycytosine, included explicit solvation using 5 water molecules in addition to the implicit (CPCM) solvation modelling. Visualization of the output geometries and their associated simulated absorption spectra utilized Avogadro, fitting each electronic transition with a Gaussian shape having a peak width of 20 nm.

2. Supplementary Results

2.1 Comparison of Absorption and Excitation Spectra

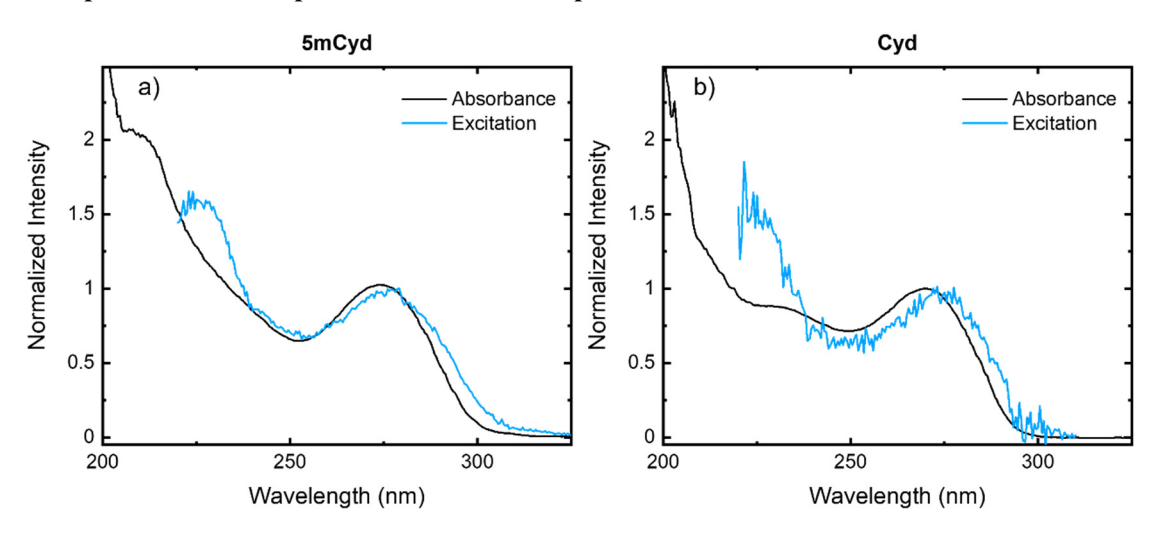


Figure S1. Comparison of normalized absorption (black) and excitation spectra (blue) of (a) 5mCyd and (b) Cyd in 16 mM phosphate buffer pH 7.4, holding emission at 330 nm and 345 nm, respectively, using a PMT voltage of 800 V with 5 nm slit widths and a scan rate of 20 nm/min.

2.2 Transient Absorption Experiments under Low Photon Density Conditions

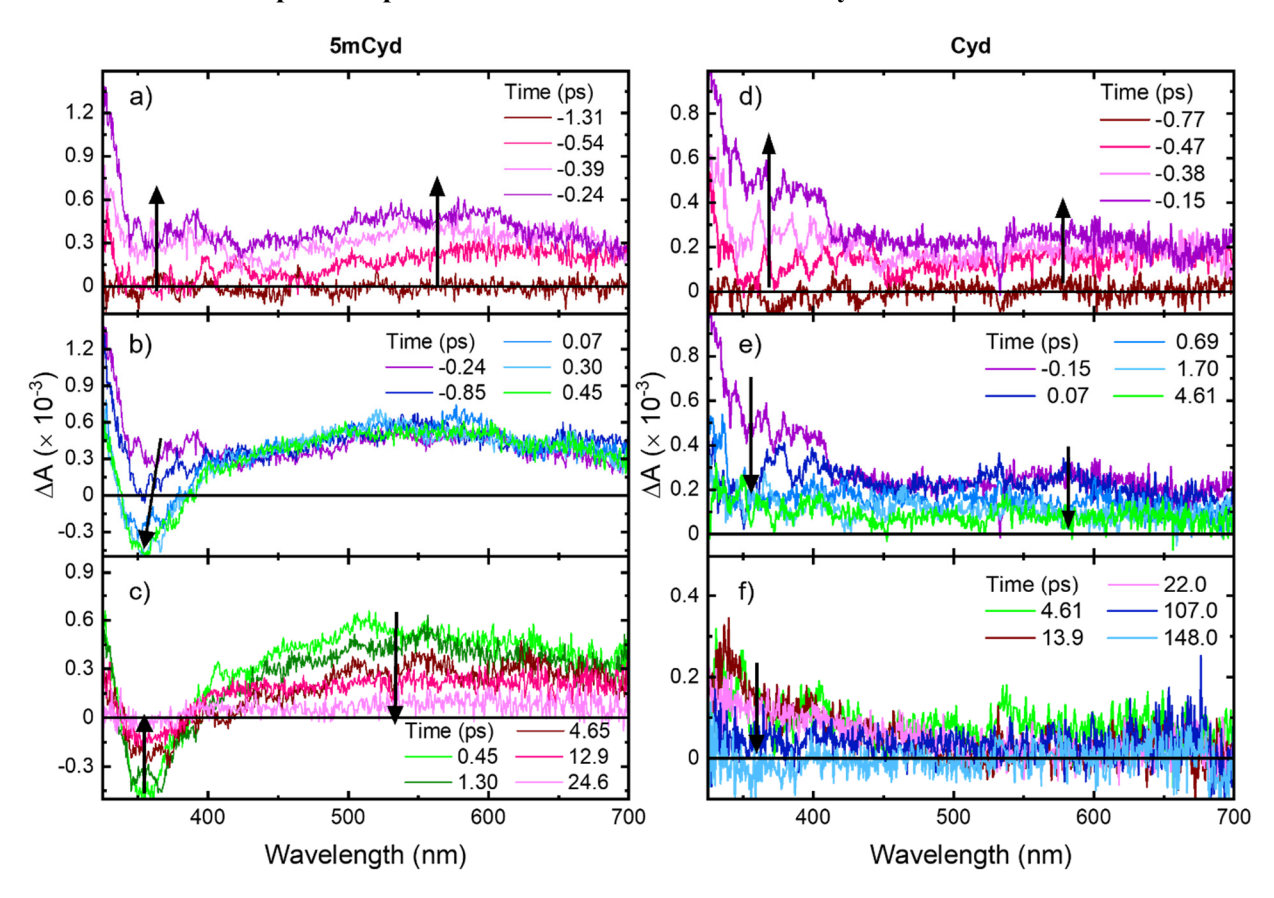


Figure S2. Selected transient absorption spectra of 5mCyd (a-c) and Cyd (d-f) in 16 mM phosphate buffer pH 7.4, following excitation at 267 nm. (Transient decay signals for 5mCyd for up to 3 ns and neat solvent are shown in Figures S5 and S6, respectively).

To eliminate the formation of hydrated electrons due to two-photon ionization of the solvent, one photon irradiation conditions were used as previously described. 5,20,23 Following excitation of 5mCyd at 267 nm, a broad transient species is observed across the entire probe window region (Figure S2a), with maxima at approximately 320 and 575 nm. During the time delays between -0.24 and 0.45 ps, a decrease and blue shift in amplitude in the UV region is observed with a maximum at ca. 350 nm, while there is no change observed in the visible region (Figure S2b). This negative amplitude ΔA signal that grows in at ca. 350 nm corresponds very well with the steady-state fluorescence emission and therefore, is assigned to stimulated emission. Finally, as shown in Figure S2c, between 0.45 and 24.6 ps, a uniform decay is observed across the entire probe region. Similarly, for Cyd, a broad transient species is observed following excitation with maxima at ca. 320 and 600 nm (Figure S2d). Between time delays of -0.15 and 4.61 ps, a decrease in amplitude is observed across the entire transient absorption spectrum to a small-amplitude signal with a maximum at ca. 370 nm (Figure S2e). This small-amplitude signal fully decays by a time delay of ca. 150 ps (Figure S2f). The full broadband transient absorption data for 5mCyd and Cyd were satisfactorily fitted with a two and three-component sequential kinetic model, respectively. The global, average lifetimes are reported in Table 1. Evolution associated difference spectra (EADS) and representative kinetic traces extracted from the global and target analyses are shown in Figures S3 and S4, respectively.

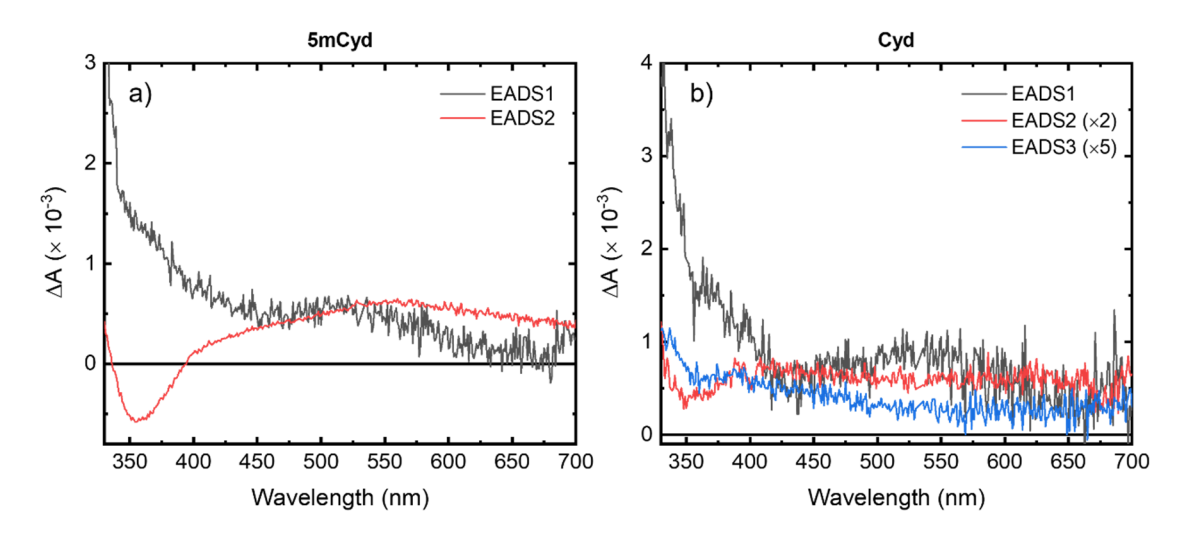


Figure S3. Evolution associated difference spectra (EADS) of 5mCyd (a) and Cyd (b) following excitation at 267 nm in phosphate buffer pH 7.4, globally fit with a three or two-component sequential model, respectively. Note, in panel b, EADS2 and EADS3 have been scaled by a factor of 2 and 5, respectively.

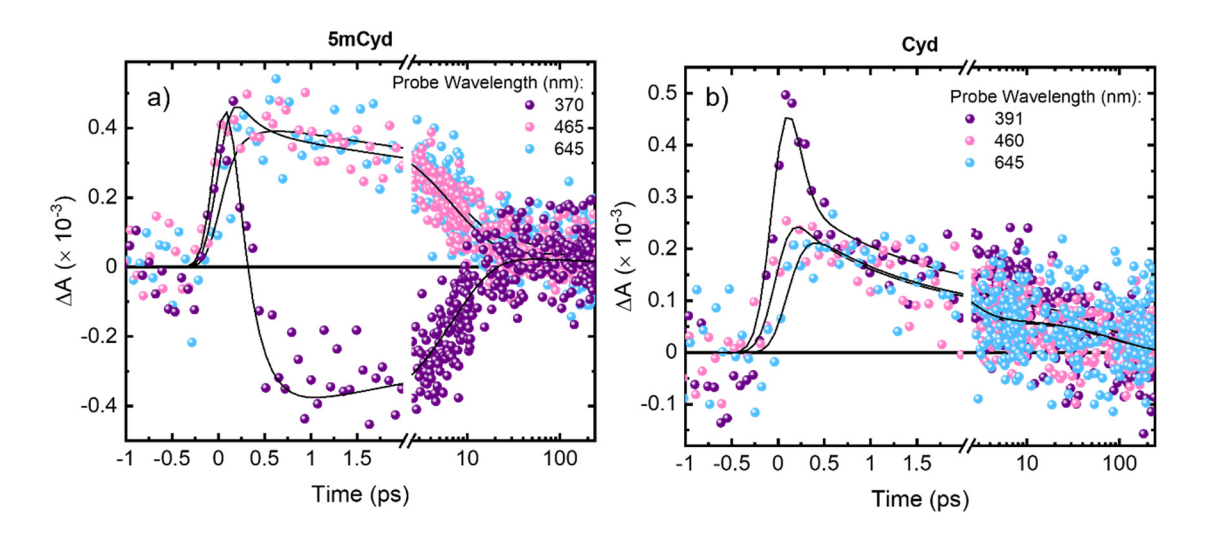


Figure S4. Representative kinetic traces of 5mCyd (left) and Cyd (right) following excitation at 267 nm in phosphate buffer pH 7.4, globally fit with a three or two-component sequential model, respectively.

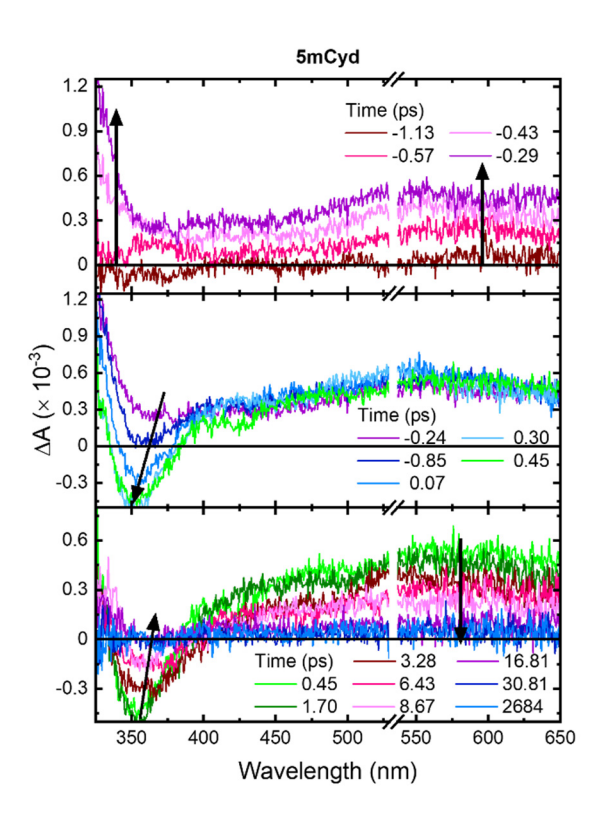


Figure S5. Selected transient absorption spectra of 5mCyd in phosphate buffer pH 7.4, following excitation at 267 nm over the full 3 ns time window. Note, the break in the abscissa to remove the overtone of the pump.

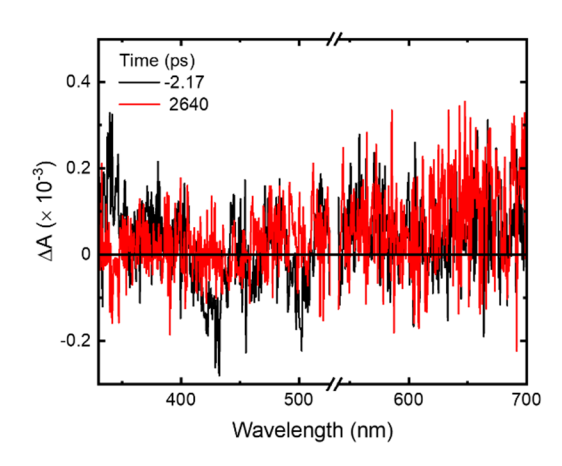


Figure S6. Select transient absorption spectra of neat phosphate buffer pH 7.4 following excitation at 267 nm, showing absence of hydrated electron species.

2.3 Transient Absorption of the Phosphate Buffer at High Photon Density Conditions

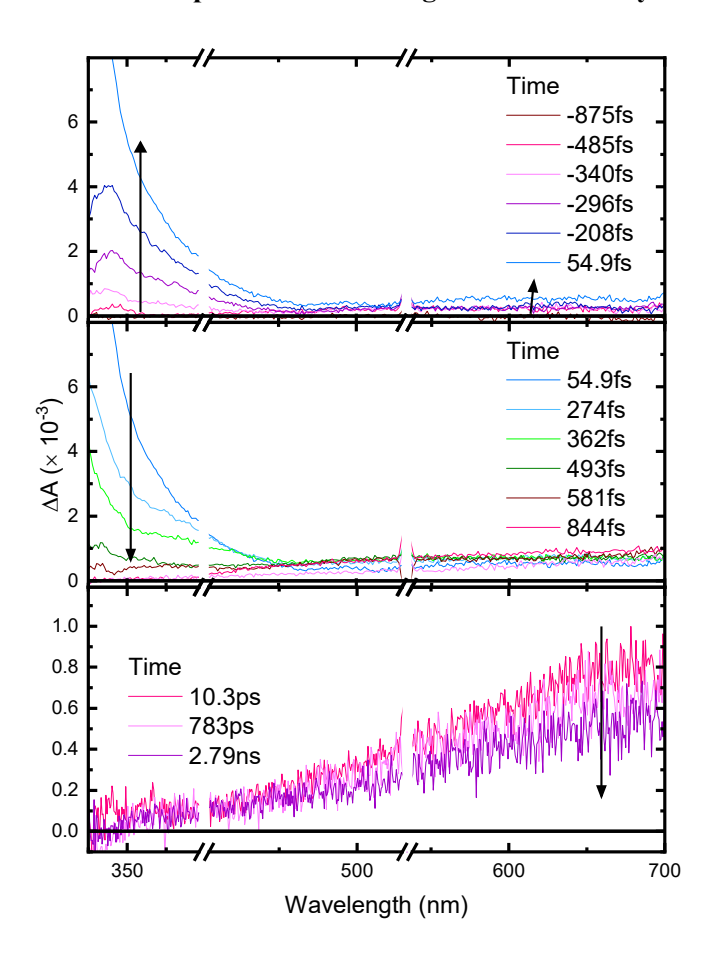


Figure S7. Transient absorption spectra of the phosphate buffer solution at pH 7.4 following laser excitation at 267 nm under high photon density.

Figure S7 shows the transient absorption spectra of phosphate buffer solution at pH 7.4 following laser excitation at 267 nm under the same high photon density conditions used in Figure 2. As described previously by Krul et al.⁵, under this higher photon density conditions, a coherent absorption band is observed at probe wavelengths below ca. 450 nm within the cross correlation of the pump and probe beams. This is followed simultaneously by the observation of the hydrated electron band resulting from the two-photon absorption of the water solvent. The correction of the transient data for 5mCyd and Cyd for the latter process is done straightforwardly using the methodology originally developed by Kohler and coworkers.²⁴ However, a correction procedure to eliminate the coherent signal from the solvent is not straightforward because it also contains the absorption of the hydrated electron band that expands all the way to 320 nm.²⁵ A correction of the transient absorption spectra for the two-photon hydrated electron band using the standard method,²⁴ leads to an over correction of the transient signal in the spectral region from ca. 320 to 450 nm.⁵ This is the reason for why it is important to use low photon density conditions when exciting at 267 nm (as shown in Figure S2 and S5 above), if the goal is to report the broadband data of a

DNA/RNA monomer (or any other chromophore) all the way from the UV to the visible. This is also the reason for why the transient data shown in Figures 2 and 3 of the main paper are "masked" or not shown below the probe wavelength of ca. 450 nm.

2.4 Partial Characterization of Primary Photoproducts

Figure S8 shows the changes in absorption spectra for 5mCyd and Cyd upon low intensity laser irradiation. The absorbance of the solutions was matched at the irradiation wavelength of 267 nm and the experiments were performed under back-to-back conditions in ultrapure water at pH 5.6. At this pH, 5mCyd exists as an equilibrium of the protonated (4.8%) and neutral keto (95.2%) forms, while Cyd exists as an equilibrium of the protonated (3.8%) and neutral keto (96.2%) forms, given the pKa values of 4.3 and 4.2 for 5mCyd²⁶ and Cyd,²⁷ respectively. We used ultrapure water at pH 5.6 for these experiments because the separation of the photoproducts using high-performance liquid chromatography (Figure S9) shown below required the use of ultrapure water at pH 5.6 as a mobile phase for optimal separation. As reported in Figure 4 in phosphate buffer solutions at pH 7.4, irradiation of both molecules at pH 5.6 results in a decrease in absorbance of the lowest energy band and of the higher energy absorption band near 200 nm. A simultaneous increase in absorbance and red shift is observed for the absorption band originally at 239 and 232 nm for 5mCyd and Cyd, respectively. In addition, isosbestic points are observed at 233 and 256 nm for 5mCyd and at 234 and 250 nm for Cyd. These changes in the absorption spectra with an increased irradiation time evidence the formation of photoproducts for both 5mCyd and Cyd (as reported in Figure 4 but at pH 7.4). 5mCyd was found to photodegrade with a rate that is three-fold smaller than Cyd in ultrapure water at pH 5.6. The increased photostability of 5mCyd compared to Cyd is consistent within the error to the experimental observations reported in the main text using phosphate buffer at pH 7.4. For Cyd, the increase in absorbance near 240 nm has previously been suggested to be due to the formation of 5,6saturated cytosine monomers, where 6-hydroxy-5,6-dihydrocytosine and β -D-ribocytidine-2', 3'-cyclic phosphate have been proposed as plausible photoproducts. ^{28–33}

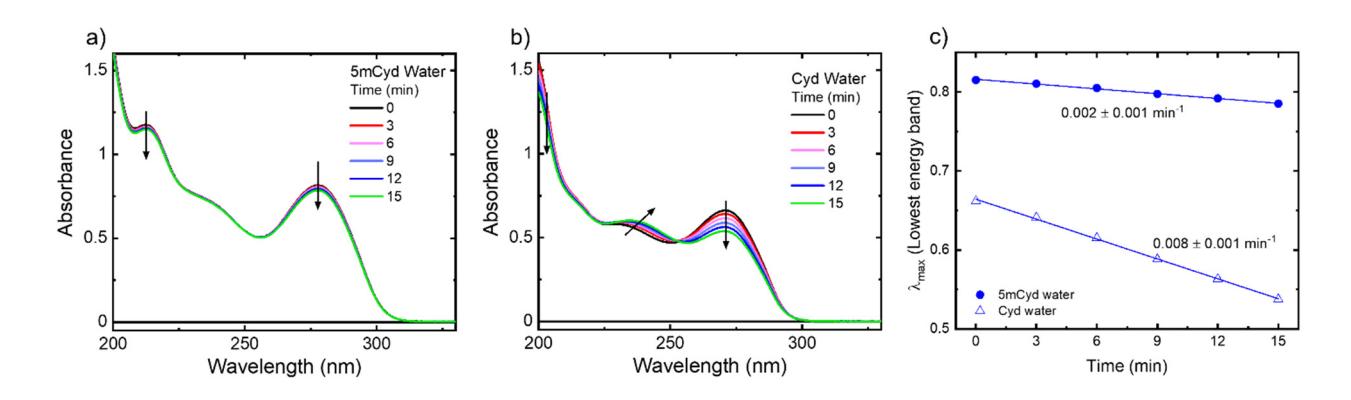


Figure S8. Photodegradation of 5mCyd (a) and Cyd (b) following low intensity laser irradiation at 267 nm in back-to-back experiments with matched optical densities at excitation wavelength in ultrapure water pH 5.6, under ambient conditions. Initial rates of photodegradation for Cyd (triangles) and 5mCyd (circles) are shown in panel c. Errors are reported as twice the standard deviation.

Figure S9 shows the separation of the photoproducts of 5mCyd and Cyd after 10 minutes of low-intensity laser irradiation at 267 nm in ultrapure water at pH 5.6. The absorption spectra of the primary

photoproducts are also shown, while those of other minor photoproducts are not shown. Using ultrapure water at pH 5.6 as the mobile phase, the parent nucleoside elutes at ca. 23 minutes for 5mCyd and at ca. 10 minutes for Cyd, well separated from the primary photoproducts. Note that the elution time of Cyd slightly changes before and after irradiation. We suggest this is due to a small change in the pH of the irradiated solution given that the irradiation experiments were performed in unbuffered, ultrapure water. The longer elution time of Cyd after irradiation (compared to before irradiation) was reproducibly observed in multiple independent irradiation experiments.

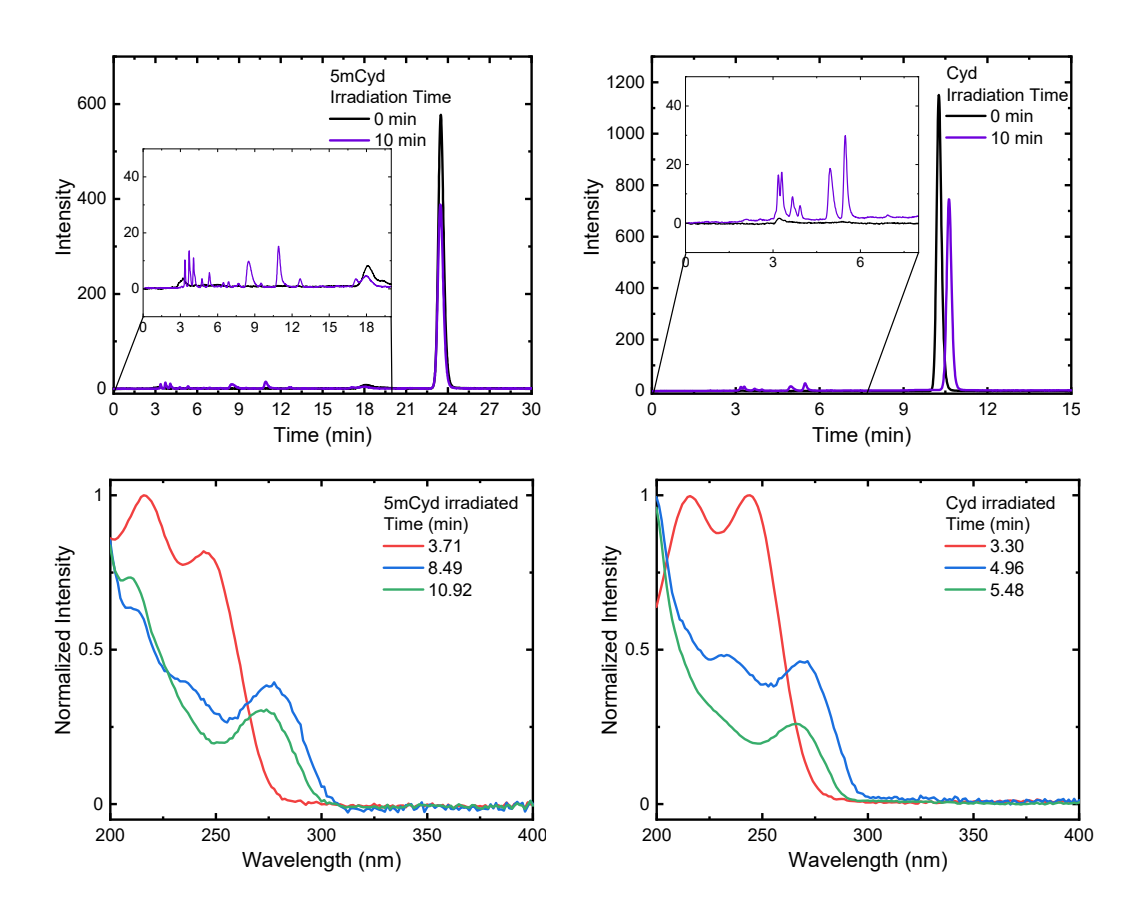


Figure S9. High-performance liquid chromatograms and absorption spectra of the primary photoproducts of 5mCyd (left) and Cyd (right) before and after low-intensity laser irradiation at 267 nm in ultrapure water, pH 5.6. Samples were freshly prepared the day of each experiment in ultrapure water (pH 5.6) to have an absorbance of 1.0 at the excitation wavelength of 267 nm.

The primary photoproducts of 5mCyd elute at ca. 3.7, 8.5, and 10.9 minutes and exhibit absorption bands with absorption below ca. 310 nm (Figure S9 bottom, left). Similarly, the primary photoproducts of Cyd elute with a retention time of ca. 3.3, 5.0, and 5.5 minutes and exhibit absorption bands below ca. 300 nm (Figure S9 bottom, right). The similar retention times and absorption spectra for the primary photoproducts of 5mCyd and Cyd suggest that their structures should be similar, but are formed in significantly less amount (i.e., ca. 3-fold) in 5mCyd than in Cyd. These observations further suggest that the excited state(s) responsible for their formation is(are) the same in both nucleosides but it is(are) populated in significantly less yield in 5mCyd than in Cyd, whether at pH of 5.6 or 7.4. The report of a

longer-lived ${}^1n_N\pi^*$ state in this Letter, and in previous works, ${}^{34\text{--}38}$ which is either formed in significantly less yield and cannot be detected in 5mCyd (Figure 2), lend indirect support to the idea that the ${}^1n_N\pi^*$ excited state participates in the formation of one or more of these photoproducts. This idea, together with the fact that the stimulated emission occurs in the same spectral region, could explain why ${}^1n_N\pi^*$ excited state in 5mCyd is not detected in Figures 2, S2, and S5. Further discussion about the possible participation of the ${}^1n_N\pi^*$ excited state in the formation of one or more photoproducts is presented below.

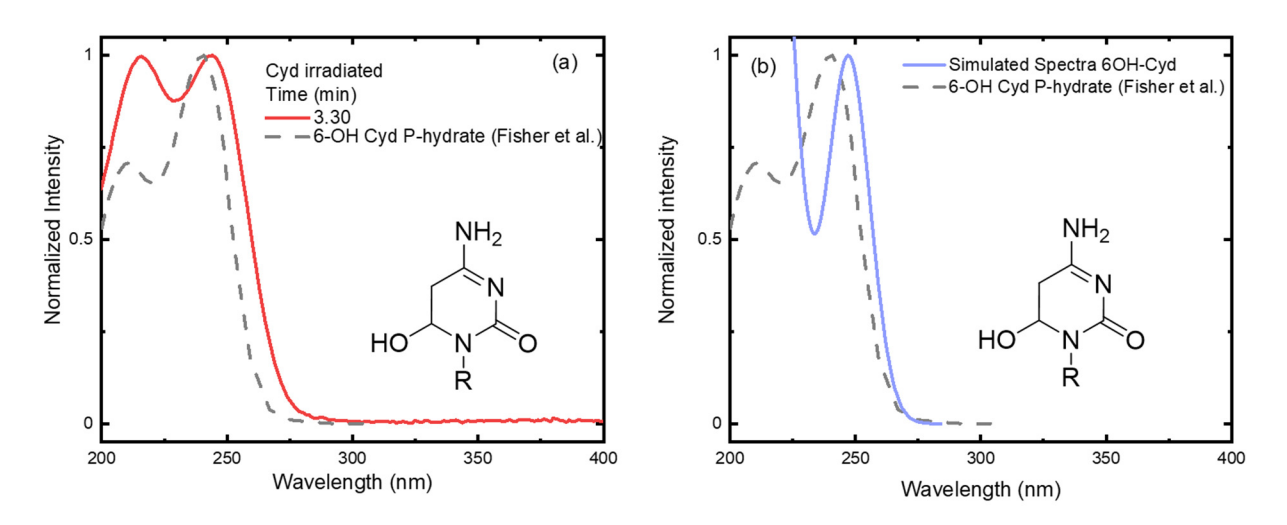


Figure S10. Comparison of 6-OH cytidine photohydrate pH 8.4 reported by Fisher and Johns³⁹ (gray, dashed) with (a) the Cyd photoproduct at time 3.30 min (red) in ultrapure water, and (b) with the simulated absorption spectrum of 6-OH cytosine (purple). The simulated spectrum was computed at the TD-PBE0-D3BJ/CPCM(+5W)/ def2-TZVPD//B3LYP_G-D3BJ/CPCM(+5W)/def2-TZVPD level of theory and shifted to the red by 16 nm.

Figure S10a compares the absorption spectrum of the Cyd photoproduct eluting at 3.3 minutes with the absorption spectrum of 6-hydroxycytidine photohydrate reported by Fisher and Johns³⁹ at pH 8.4. Both absorption spectra closely resemble each other. The exception is the high-energy absorption band around ca. 210 nm, which has somewhat lower intensity in the 6-hydroxycytidine photoproduct compared to the photoproduct eluting at 3.30 min. We have also optimized the ground state of 6-hydroxycytosine in a hybrid 5 explicit waters (5W) with implicit CPCM water solvation model and simulated its absorption spectrum at the TD-PBE0-D3BJ/CPCM(+5W)/def2-TZVPD//B3LYP_G-D3BJ/CPCM(+5W)/def2-TZVPD level of theory. The simulated absorption spectrum compares fairly well with the absorption spectra of the 6hydroxycytidine photoproduct (and that eluting at 3.3 min). Once again, the exception is with the highenergy band around 210 nm that has significantly more intensity in the simulated spectrum for 6hydroxycytosine (Figure S10b). Taking into consideration that the absorption of the photoproduct eluting at 3.3 min was collected using a photodiode array detector of a HPLC instrument and at pH of 5.6, while that of the 6-hydroxycytidine photoproduct was recorded at pH of 8.4, presumably in a UV-vis spectrophotometer, we argue that the agreement between both spectra is quite satisfactory. Collectively, the experimental and computational data reported herein suggest that the photoproduct eluting at 3.3 min is likely the 6-hydroxycytidine photoproduct.

In 1972, Burr et al.⁴⁰ presented experimental evidence that the Cyd photohydrates are not formed from the fluorescence excited singlet state or the triplet excited state but likely from a 1 n π^{*} excited state or

a singlet excited water-Cyd complex. Recently, Szabla and coworkers⁴¹ investigate the formation of the 6-hydroxycytidine and other photoproducts computationally using cytosine (C) and 1-methylcytosine (1mC) complexed with two explicit water molecules at the CC2 and MR-CISD levels of theory. The authors concluded that a $^1n\pi^*$ state primarily associated with a n_N molecular orbital and characterized by pronounced water-to-C or water-to-1mC charge transfer and a strong water-N3 interaction, can give rise to the formation of 6-hydroxycytidine, oxazolidinone, and α -uridine photoproducts. The experimental and computational results by Burr and Szabla lend further support to our proposal that the $^1n_N\pi^*$ excited state give rise to the formation of 6-hydroxycytidine and likely to others of the primary photoproducts of Cyd (and conceivably in 5mCyd) in aqueous solution, possibly through the reaction mechanism described Szabla and coworkers.⁴¹ See, Figures 5 and 6, and associated discussion in their paper.⁴¹

2.5 Photodegradation Rates in Acetonitrile

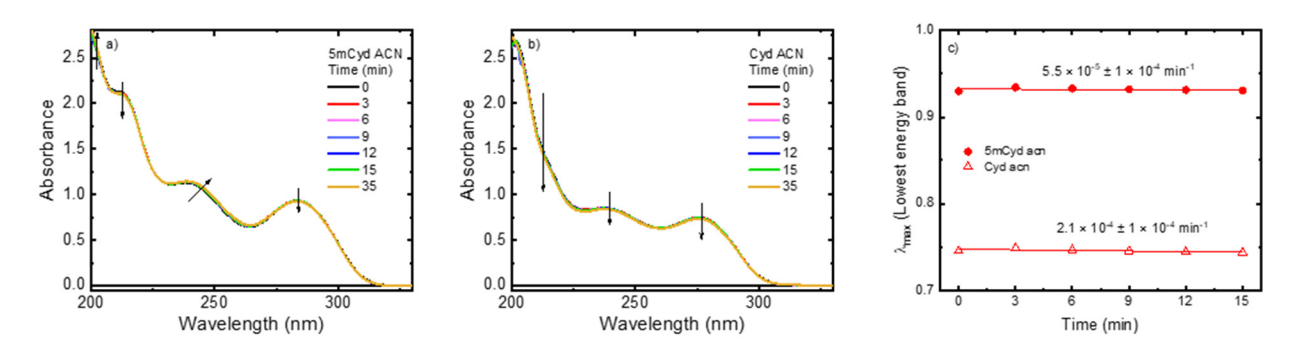


Figure S11. Photodegradation of 5mCyd (a) and Cyd (b) following low intensity laser irradiation at 267 nm in back-to-back experiments in dry (<0.01% water) acetonitrile (ACN), under ambient conditions. Initial rates of photodegradation for Cyd (red pen triangles) and 5mCyd (red circles) are shown in panel (c). Errors are reported as twice the standard deviation.

To further supports the idea that 6-hydroxycytidine and other primary photoproducts are formed from an $^1n_N\pi^*$ excited state reacting with a water molecule, Figure S11 presents the changes in the absorption spectra for 5mCyd and Cyd following low intensity laser irradiation at 267 nm in dry (< 0.01% water) acetonitrile at ambient conditions. The corresponding photodegradation rates are also reported in panel (c). The photoreactivity of both 5mCyd and Cyd decreases by two to three orders of magnitude relative to the experiments performed in aqueous solution. This observation strongly support the idea that water molecules play a key role in the formation of the main photoproducts, as proposed above and predicted by quantum chemical calculations.⁴¹

2.6 Other Primary Photoproducts

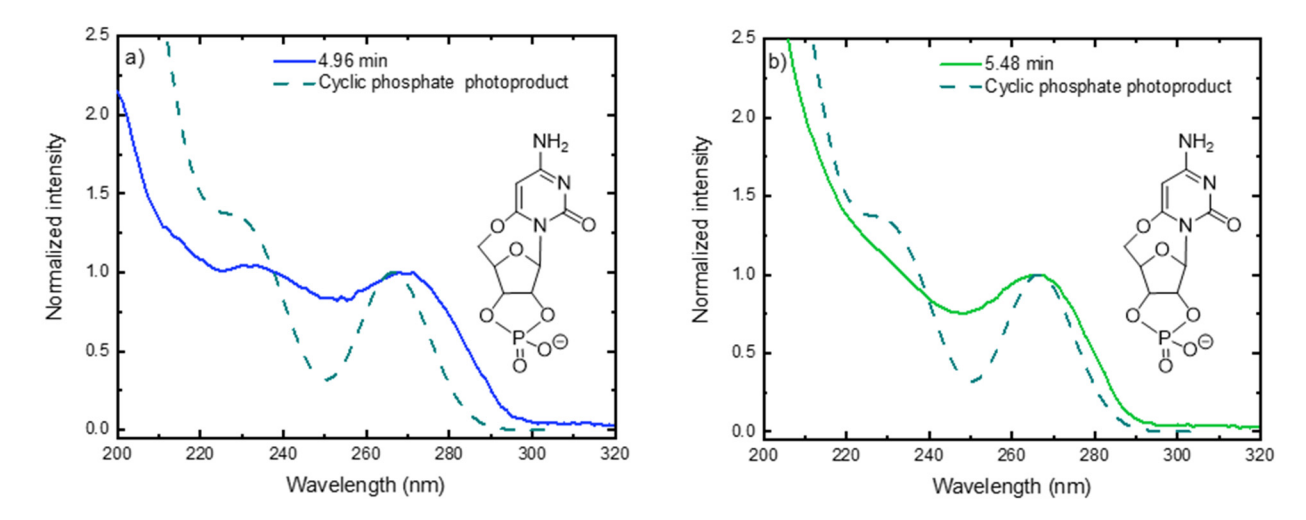


Figure S12. Comparison of the HPLC separated photoproduct of Cyd following irradiation at 267 nm at elution times of 4.96 min (a, blue solid line) and 5.48 min (b, green solid line) with the simulated spectrum of the hypothesized intermediate on UV irradiation of β -d-ribocytidine-2',3'-cyclic phosphate suggested by Powner et al.³¹ and Todd et al.⁴² (teal, dashed line). The simulated absorption spectrum was computed in water at the TD-PBE0-D3BJ/CPCM/def2-TZVPD// B3LYP_G-D3BJ/CPCM/def2-TZVPD level of theory and red shifted by 20 nm.

Figure S12 compares the absorption spectra of the photoproducts eluting at 4.96 and 5.48 min with the simulated absorption spectrum of the β -d-ribocytidine-2',3'-cyclic phosphate intermediate suggested by Powner et al.³¹ and Todd et al.⁴² Unfortunately, the experimental absorption spectrum of β -d-ribocytidine-2',3'-cyclic phosphate is not reported by the authors. The agreement of the experimental spectra of the photoproducts eluting at 4.96 and 5.48 min (recorded at pH 5.6 and with the HPLC photodiode array detector) with the calculated spectrum is reasonable, particularly for the photoproduct eluting at 4.96 min. However, we remark that more experimental and computational work is necessary to characterize these photoproducts unequivocally.

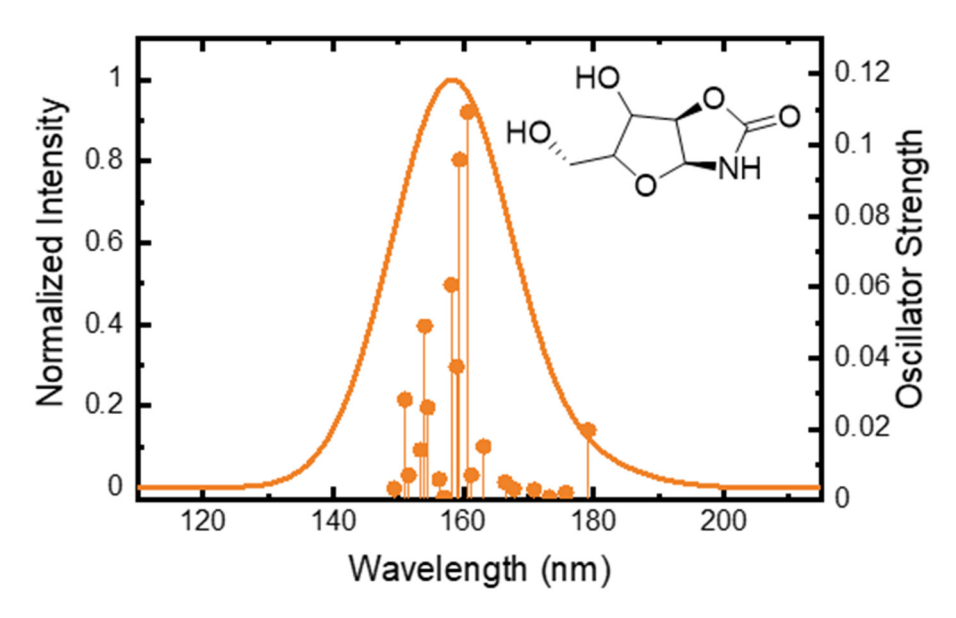


Figure S13. Simulated absorption spectrum of the oxazolidinone photoproduct^{31,43–46} in water at the TD-PBE0-D3BJ/CPCM/def2-TZVPD//B3LYP_G-D3BJ/CPCM/def2-TZVPD level of theory.

Finally, Figure S13 reports the simulated absorption spectrum of the oxazolidinone photoproduct in water. Sutherland and coworkers characterized oxazolidinone as a major photoproduct of α -Cyd. $^{31,43-46}$ This photoproduct is predicted to absorb below 200 nm, which is below the detection cutoff of the photodiode array detector of the HPLC used in this study. Its absorption spectrum is provided here for completeness.

2.7 On the Participation of the ${}^{1}n_{0}\pi^{*}$ State

Figure S14 compares the EADS3 reported in Figure S3b both with the absorption spectrum of the 1 n_N π^* state and with the absorption spectrum of a linear combination of the 1 n_N π^* and 1 n_O π^* states. While the absorption spectrum of the ${}^{1}n_{N}\pi^{*}$ state compares satisfactorily well with the EADS3, a 50%:50% linear combination of the absorption spectrum of the ${}^{1}n_{N}\pi^{*}$ and either the planar or twisted ${}^{1}n_{O}\pi^{*}$ states also seems to be in fair agreement. Note that the predicted absorption spectra of the planar and twisted ${}^{1}n_{0}\pi^{*}$ minima are practically identical and, hence, do not affect the linear combination. We cannot rule out a minor participation of the ${}^{1}n_{0}\pi^{*}$ state in the experimental data. However, we note that if both ${}^{1}n_{0}\pi^{*}$ and ${}^{1}n_{0}\pi^{*}$ excited states were populated in Cyd, their excited state decay lifetimes would be expected to be different from each other. Because the absorption spectrum of the ${}^{1}n_{0}\pi^{*}$ state is predicted to have more intensity around 330 nm, while that of ${}^{1}n_{N}\pi^{*}$ state is predicted to have more intensity around 420 nm and 550 nm (i.e., relative to each other), we have normalized the decay traces at these three probe wavelengths (see, Figure S15). As can be seeing in Figure S15, the dynamics are practically identical within the signal-tonoise and decay in lock step with each other for kinetic traces at 330 nm and 420 nm, however the dynamics are vastly different at 550 nm. This provides strong experimental evidence that the EADS3 is primarily associated to a single transient species (the absorption of the ${}^{1}n_{N}\pi^{*}$ state) and not to a combination of two or more transient species. This idea is further supported by quantum chemical calculations for cytosine and 1-methylcytosine that includes explicit water molecules, 41 which have shown that the $^1n_N\pi^*$ minimum is lower in energy than the ${}^{1}n_{0}\pi^{*}$ minima, and the ${}^{1}n_{0}\pi^{*}$ state is also significantly higher in energy in the Franck-Condon region, and should not be populated to any major extent upon excitation at 267 nm.

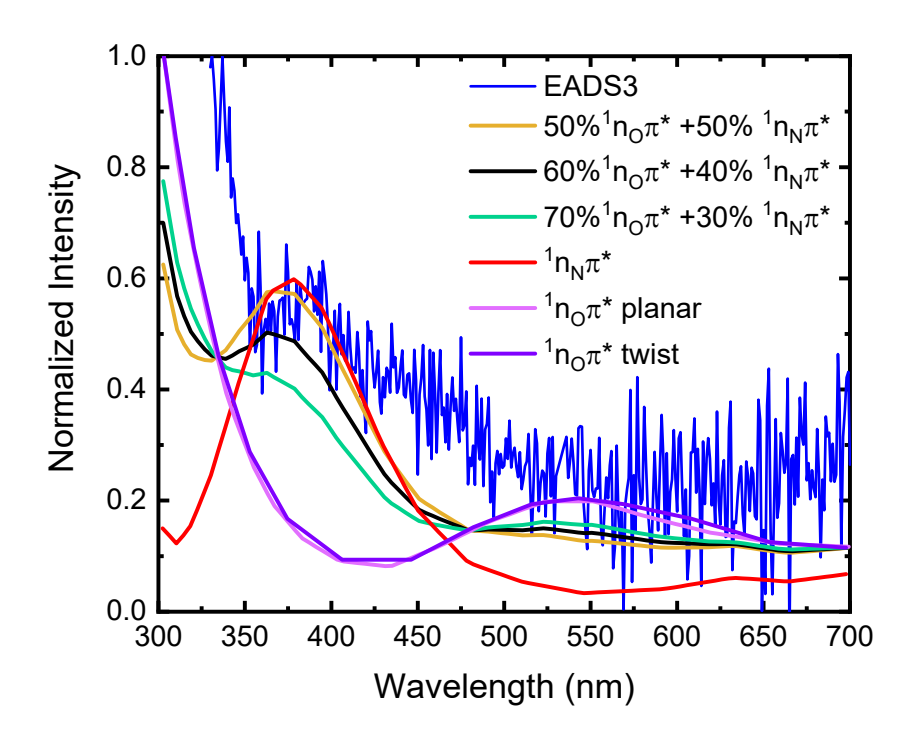


Figure S14. Comparison of experimentally obtained Cyd EADS 3 (blue) from the low photon density transient absorption data with linear combinations of the ${}^{1}n_{N}\pi^{*}$ and ${}^{1}n_{O}\pi^{*}$ computed spectra reproduced from Pepino et al.⁴⁷

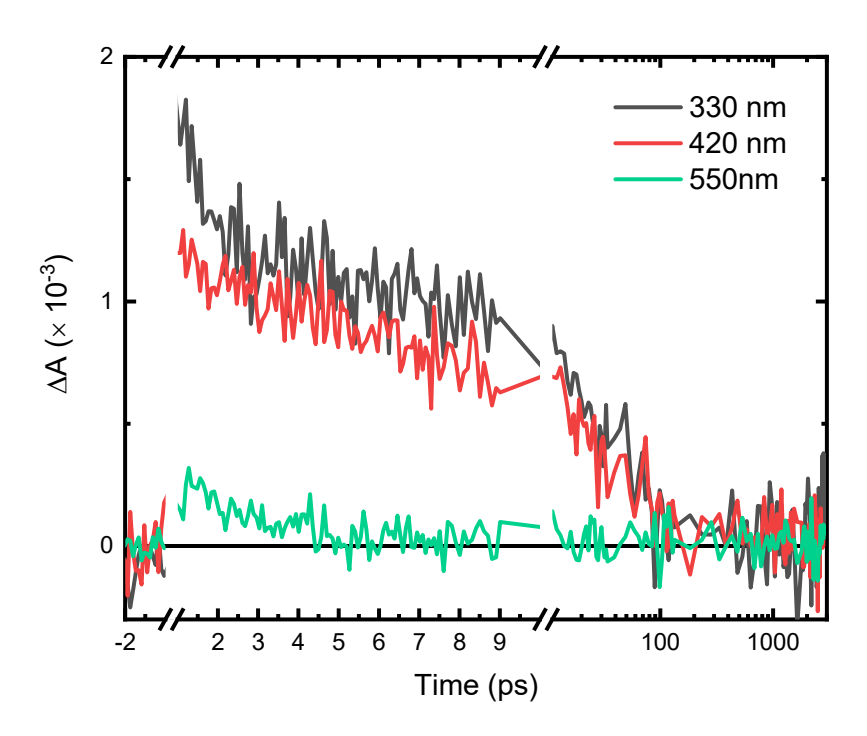


Figure S15. Representative kinetic traces of Cyd from high photon density transient data. For ease of comparison traces at 320 and 420 nm were normalized at ca. 5 ps, however due to the significantly smaller intensity of the signal at 550 nm this trace was plotted without normalization as to not highlight the noise of the data. Note the break around time zero, which is masking a strong coherent signal from the solvent at 330 nm.

Supporting References

- (1) Lakowicz, J. R. *Principles of Fluorescence Spectroscopy*; Lakowicz, J. R., Ed.; Springer US: Boston, MA, **2006**. https://doi.org/10.1007/978-0-387-46312-4.
- Onidas, D.; Markovitsi, D.; Marguet, S.; Sharonov, A.; Gustavsson, T. Fluorescence Properties of DNA Nucleosides and Nucleotides: A Refined Steady-State and Femtosecond Investigation. *J. Phys. Chem. B* **2002**, *106* (43), 11367–11374. https://doi.org/10.1021/jp026063g.
- (3) Strickler, S. J.; Berg, R. A. Relationship between Absorption Intensity and Fluorescence Lifetime of Molecules. *J. Chem. Phys.* **1962**, *37* (4), 814–822. https://doi.org/10.1063/1.1733166.
- (4) Cohen, B.; Crespo-Hernández, C. E.; Kohler, B. Strickler–Berg Analysis of Excited Singlet State Dynamics in DNA and RNA Nucleosides. *Faraday Discuss.* **2004**, *127*, 137–147. https://doi.org/10.1039/B316939A.
- (5) Krul, S. E.; Hoehn, S. J.; Feierabend, K. J.; Crespo-Hernández, C. E. Excited State Dynamics of 7-Deazaguanosine and Guanosine 5'-Monophosphate. *J. Chem. Phys.* **2021**, *154* (7), 075103. https://doi.org/10.1063/5.0038123.
- (6) Reichardt, C.; Vogt, R. A.; Crespo-Hernández, C. E. On the Origin of Ultrafast Nonradiative Transitions in Nitro-Polycyclic Aromatic Hydrocarbons: Excited-State Dynamics in 1-Nitronaphthalene. *J. Chem. Phys.* **2009**, *131* (22), 224518. https://doi.org/10.1063/1.3272536.
- (7) Pollum, M.; Jockusch, S.; Crespo-Hernández, C. E. 2,4-Dithiothymine as a Potent UVA Chemotherapeutic Agent. *J. Am. Chem. Soc.* **2014**, *136* (52), 17930–17933. https://doi.org/10.1021/ja510611j.
- (8) Brister, M. M.; Crespo-Hernández, C. E. Excited-State Dynamics in the RNA Nucleotide Uridine 5'-Monophosphate Investigated Using Femtosecond Broadband Transient Absorption Spectroscopy. *J. Phys. Chem. Lett.* **2019**, *10* (9), 2156–2161. https://doi.org/10.1021/acs.jpclett.9b00492.
- (9) Snellenburg, J. J.; Laptenok, S.; Seger, R.; Mullen, K. M.; van Stokkum, I. H. M. Glotaran: A Java-Based Graphical User Interface for the R Package TIMP. *J. Stat. Softw.* **2012**, *49* (3), 1–22. https://doi.org/10.18637/jss.v049.i03.
- (10) Van Stokkum, I. H. M.; Larsen, D. S.; Van Grondelle, R. Global and Target Analysis of Time-Resolved Spectra. *Biochimica et Biophysica Acta Bioenergetics*. July 9, 2004, pp 82–104. https://doi.org/10.1016/j.bbabio.2004.0411.
- (11) van Stokkum, I. H. M.; Larsen, D. S.; van Grondelle, R. Erratum to "Global and Target Analysis of Time-Resolved Spectra." *Biochim. Biophys. Acta Bioenerg.* **2004**, *1658* (3), 262. https://doi.org/10.1016/j.bbabio.2004.08.005.
- (12) Neese, F.; Wennmohs, F.; Becker, U.; Riplinger, C. The ORCA Quantum Chemistry Program Package. *J. Chem. Phys.* **2020**, *152* (22), 224108. https://doi.org/10.1063/5.0004608.
- (13) Becke, A. D. Density-Functional Exchange-Energy Approximation with Correct Asymptotic Behavior. *Phys. Rev. A* **1988**, *38* (6), 3098–3100. https://doi.org/10.1103/PhysRevA.38.3098.
- (14) Lee, C.; Yang, W.; Parr, R. G. Development of the Colle-Salvetti Correlation-Energy Formula into a Functional of the Electron Density. *Phys. Rev. B* **1988**, *37* (2), 785–789. https://doi.org/10.1103/PhysRevB.37.785.
- (15) Perdew, J. P.; Ernzerhof, M.; Burke, K. Rationale for Mixing Exact Exchange with Density

- Functional Approximations. *J. Chem. Phys.* **1996**, *105* (22), 9982–9985. https://doi.org/10.1063/1.472933.
- (16) Rappoport, D.; Furche, F. Property-Optimized Gaussian Basis Sets for Molecular Response Calculations. *J. Chem. Phys.* **2010**, *133* (13), 134105. https://doi.org/10.1063/1.3484283.
- (17) Weigend, F.; Ahlrichs, R. Balanced Basis Sets of Split Valence, Triple Zeta Valence and Quadruple Zeta Valence Quality for H to Rn: Design and Assessment of Accuracy. *Phys. Chem. Chem. Phys.* **2005**, *7* (18), 3297. https://doi.org/10.1039/b508541a.
- (18) Grimme, S.; Antony, J.; Ehrlich, S.; Krieg, H. A Consistent and Accurate Ab Initio Parametrization of Density Functional Dispersion Correction (DFT-D) for the 94 Elements H-Pu. *J. Chem. Phys.* **2010**, *132* (15), 154104. https://doi.org/10.1063/1.3382344.
- (19) Grimme, S.; Ehrlich, S.; Goerigk, L. Effect of the Damping Function in Dispersion Corrected Density Functional Theory. *J. Comput. Chem.* **2011**, *32* (7), 1456–1465. https://doi.org/10.1002/jcc.21759.
- (20) Hoehn, S. J.; Krul, S. E.; Skory, B. J.; Crespo-Hernández, C. E. Increased Photostability of the Integral mRNA Vaccine Component N1-Methylpseudouridine Compared to Uridine. *Chem. A Eur. J.* **2022**, *28* (6), e202103667. https://doi.org/10.1002/chem.202103667.
- (21) Neese, F. An Improvement of the Resolution of the Identity. *J. Comput. Chem.* **2003**, *24* (14), 1740–1747.
- (22) Izsák, R.; Neese, F. An Overlap Fitted Chain of Spheres Exchange Method. *J. Chem. Phys.* **2011**, *135* (14), 144105. https://doi.org/10.1063/1.3646921.
- (23) Krul, S. E.; Costa, G. J.; Hoehn, S. J.; Valverde, D.; Oliveira, L. M. F.; Borin, A. C.; Crespo-Hernández, C. E. Resolving Ultrafast Photoinitiated Dynamics of the Hachimoji 5-aza-7-deazaguanine Nucleobase: Impact of Synthetically Expanding the Genetic Alphabet. *Photochem. Photobiol.* **2023**, *99* (2), 693–705. https://doi.org/10.1111/php.13688.
- (24) Crespo-Hernández, C. E.; Kohler, B. Influence of Secondary Structure on Electronic Energy Relaxation in Adenine Homopolymers. *J. Phys. Chem. B* **2004**, *108* (30), 11182–11188. https://doi.org/10.1021/jp0496046.
- (25) Thomsen, C. L.; Madsen, D.; Keiding, S. R.; Thøgersen, J.; Christiansen, O. Two-Photon Dissociation and Ionization of Liquid Water Studied by Femtosecond Transient Absorption Spectroscopy. *J. Chem. Phys.* **1999**, *110* (7), 3453–3462. https://doi.org/10.1063/1.478212.
- (26) Fox, J. J.; Van Praag, D.; Wempen, I.; Doerr, I. L.; Cheong, L.; Knoll, J. E.; Eidinoff, M. L.; Bendich, A.; Brown, G. B. Thiation of Nucleosides. II. Synthesis of 5-Methyl-2'-Deoxycytidine and Related Pyrimidine Nucleosides 1. *J. Am. Chem. Soc.* **1959**, *81* (1), 178–187. https://doi.org/10.1021/ja01510a042.
- (27) Shugar, D.; Fox, J. J. Spectrophotometric Studies Op Nucleic Acid Derivatives and Related Compounds as a Function of pH. *Biochim. Biophys. Acta* **1952**, *9*, 199–218. https://doi.org/10.1016/0006-3002(52)90147-9.
- (28) Sinsheimer, R. L. The Photochemistry of Cytidylic Acid. *Radiat. Res.* **1957**, *6* (2), 121–125. https://doi.org/10.2307/3570592.
- (29) Wierzchowski, K. L.; Shugar, D. Photochemistry of Cytosine Nucleosides and Nucleotides. *Biochim. Biophys. Acta* **1957**, *25*, 355–364. https://doi.org/10.1016/0006-3002(57)90479-1.

- (30) Wang, S. Y. Ultra-Violet Irradiation of 1,3-Dimethylthymine. *Nature* **1959**, *184* (4688), BA59–BA61. https://doi.org/10.1038/184059a0b.
- (31) Powner, M. W.; Gerland, B.; Sutherland, J. D. Synthesis of Activated Pyrimidine Ribonucleotides in Prebiotically Plausible Conditions. *Nature* **2009**, *459* (7244), 239–242. https://doi.org/10.1038/nature08013.
- (32) Burr, J. G. Nucleic Acid Derivatives. In *Thin-Layer Chromatography, Revised And Expanded*; CRC Press, **1999**; Vol. 6, pp 212–217. https://doi.org/10.1201/9780203910214.ch20.
- (33) Wang, S. Y. *Photochemistry and Photobiology of Nucleic Acids*; Academic Press: New York, **1976**. https://doi.org/10.1016/B978-0-12-734601-4.X5001-0.
- (34) Ma, C.; Cheng, C. C.-W.; Chan, C. T.-L.; Chan, R. C.-T.; Kwok, W.-M. Remarkable Effects of Solvent and Substitution on the Photo-Dynamics of Cytosine: A Femtosecond Broadband Time-Resolved Fluorescence and Transient Absorption Study. *Phys. Chem. Chem. Phys.* 2015, 17 (29), 19045–19057. https://doi.org/10.1039/C5CP02624E.
- (35) Barbatti, M.; Aquino, A. J. A.; Szymczak, J. J.; Nachtigallová, D.; Hobza, P.; Lischka, H. Relaxation Mechanisms of UV-Photoexcited DNA and RNA Nucleobases. *Proc. Natl. Acad. Sci.* **2010**, *107* (50), 21453–21458. https://doi.org/10.1073/pnas.1014982107.
- (36) Keane, P. M.; Wojdyla, M.; Doorley, G. W.; Watson, G. W.; Clark, I. P.; Greetham, G. M.; Parker, A. W.; Towrie, M.; Kelly, J. M.; Quinn, S. J. A Comparative Picosecond Transient Infrared Study of 1-Methylcytosine and 5'-dCMP That Sheds Further Light on the Excited States of Cytosine Derivatives. *J. Am. Chem. Soc.* **2011**, *133* (12), 4212–4215. https://doi.org/10.1021/ja1106089.
- (37) Quinn, S.; Doorley, G. W.; Watson, G. W.; Cowan, A. J.; George, M. W.; Parker, A. W.; Ronayne, K. L.; Towrie, M.; Kelly, J. M. Ultrafast IR Spectroscopy of the Short-Lived Transients Formed by UV Excitation of Cytosine Derivatives. *Chem. Commun.* **2007**, No. 21, 2130–2132. https://doi.org/10.1039/b703344c.
- (38) Miura, Y.; Yamamoto, Y. I.; Karashima, S.; Orimo, N.; Hara, A.; Fukuoka, K.; Ishiyama, T.; Suzuki, T. Formation of Long-Lived Dark States during Electronic Relaxation of Pyrimidine Nucleobases Studied Using Extreme Ultraviolet Time-Resolved Photoelectron Spectroscopy. *J. Am. Chem. Soc.* **2023**, *145* (6), 3369–3381. https://doi.org/10.1021/jacs.2c09803.
- (39) Fisher, G. J.; Johns, H. E. Pyrimidine Photohydrates. In *Photochemistry and Photobiology of Nucleic Acids*; Wang, S. Y., Ed.; Academic Press, **1976**; 169–224. https://doi.org/https://doi.org/10.1016/B978-0-12-734601-4.50010-0.
- (40) Burr, J. G.; Park, E. H.; Chan, A. Nature of the Reactive Species in the Photohydration of Uracil and Cytosine Derivatives. *J. Am. Chem. Soc.* **1972**, *94* (16), 5866–5872. https://doi.org/10.1021/ja00771a054.
- (41) Szabla, R.; Kruse, H.; Šponer, J.; Góra, R. W. Water-Chromophore Electron Transfer Determines the Photochemistry of Cytosine and Cytidine. *Phys. Chem. Chem. Phys.* **2017**, *19* (27), 17531–17537. https://doi.org/10.1039/c7cp02635h.
- (42) Todd, Z. R.; Fahrenbach, A. C.; Ranjan, S.; Magnani, C. J.; Szostak, J. W.; Sasselov, Di. D. Ultraviolet-Driven Deamination of Cytidine Ribonucleotides Under Planetary Conditions. *Astrobiology* **2020**, *20* (7), 878–888. https://doi.org/10.1089/ast.2019.2182.
- (43) Anastasi, C.; Crowe, M. A.; Powner, M. W.; Sutherland, J. D. Direct Assembly of Nucleoside Precursors from Two- and Three-Carbon Units. *Angew. Chemie* **2006**, *118* (37), 6322–6325.

- https://doi.org/10.1002/ange.200601267.
- (44) Anastasi, C.; Crowe, M. A.; Sutherland, J. D. Two-Step Potentially Prebiotic Synthesis of α-D-Cytidine-5'- Phosphate from D-Glyceraldehyde-3-Phosphate. *J. Am. Chem. Soc.* **2007**, *129* (1), 24–25. https://doi.org/10.1021/ja066495v.
- (45) Powner, M. W.; Anastasi, C.; Crowe, M. A.; Parkes, A. L.; Raftery, J.; Sutherland, J. D. On the Prebiotic Synthesis of Ribonucleotides: Photoanomerisation of Cytosine Nucleosides and Nucleotides Revisited. *ChemBioChem* **2007**, *8* (10), 1170–1179. https://doi.org/10.1002/cbic.200700098.
- (46) Powner, M. W.; Sutherland, J. D. Potentially Prebiotic Synthesis of Pyrimidine β-D-Ribonucleotides by Photoanomerization/Hydrolysis of α-D-Cytidine-2'-Phosphate. *ChemBioChem* 2008, 9 (15), 2386–2387. https://doi.org/10.1002/cbic.200800391.
- (47) Pepino, A. J.; Segarra-Martí, J.; Nenov, A.; Rivalta, I.; Improta, R.; Garavelli, M. UV-Induced Long-Lived Decays in Solvated Pyrimidine Nucleosides Resolved at the MS-CASPT2/MM Level. *Phys. Chem. Chem. Phys.* **2018**, *20* (10), 6877–6890. https://doi.org/10.1039/C7CP08235E.